Article

Structure

The Preprotein Binding Domain of SecA Displays Intrinsic Rotational Dynamics

Graphical Abstract

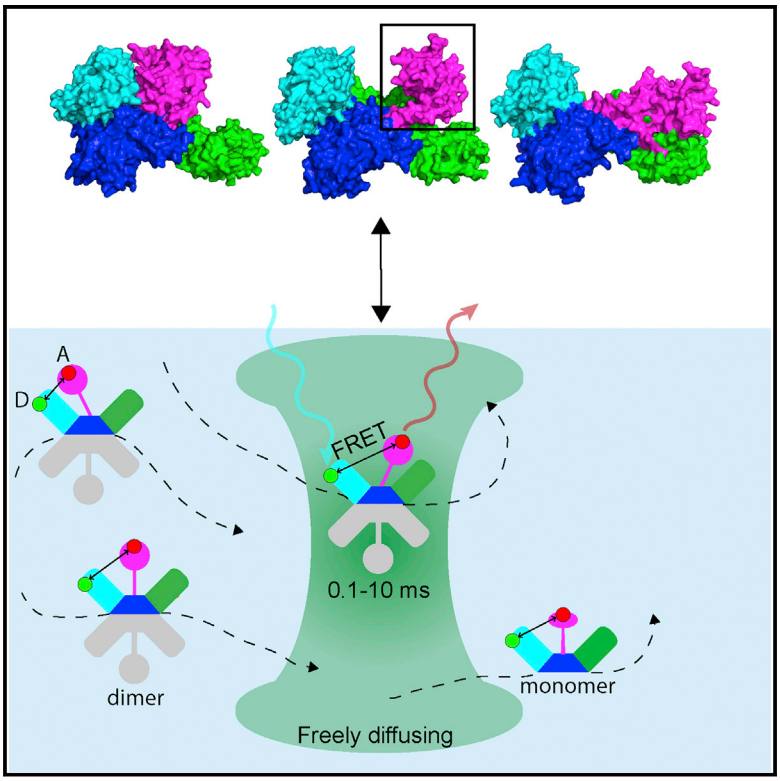

Authors

Niels Vandenberk, Spyridoula Karamanou, Athina G. Portaliou, Valentina Zorzini, Johan Hofkens, Jelle Hendrix, Anastassios Economou

Correspondence

jelle.hendrix@uhasselt.be (J.H.), tassos.economou@kuleuven.be (A.E.)

In Brief

Vandenberk et al. determine that the preprotein binding domain of SecA, the protein translocase motor, swivels around the stem that connects it to the rest of SecA. Single-molecule FRET determined several distinct states in native dimeric and monomeric SecA. Possible contributions of these motions to SecA catalysis are discussed.

Highlights

- The preprotein binding domain of SecA is mobile in solution
- PBD swivels around its stem to acquire 3–4 distinct states
- Monomerization, but not nucleotides, regulate PBD swiveling
- smFRET provides unique dynamics analysis of SecA

Vandenberk et al., 2019, Structure *27*, 1–12
January 2, 2019
https://doi.org/10.1016/j.str.2018.10.006

CellPress

Please cite this article in press as: Vandenberk et al., The Preprotein Binding Domain of SecA Displays Intrinsic Rotational Dynamics, Structure (2018), https://doi.org/10.1016/j.str.2018.10.006

Structure
Article

The Preprotein Binding Domain of SecA Displays Intrinsic Rotational Dynamics

Niels Vandenberk,[1] Spyridoula Karamanou,[2] Athina G. Portaliou,[2] Valentina Zorzini,[2] Johan Hofkens,[1] Jelle Hendrix,[1,3,*] and Anastassios Economou[2,4,*]

[1]KU Leuven, Department of Chemistry, Division for Molecular Imaging and Photonics, Laboratory for Photochemistry and Spectroscopy, Celestijnenlaan 200F, B-3001 Leuven, Belgium

[2]KU Leuven, Department of Microbiology and Immunology, Rega Institute for Medical Research, Laboratory for Molecular Bacteriology, Herestraat 49, Gasthuisberg Campus, B-3000 Leuven, Belgium

[3]Dynamic Bioimaging Lab, Advanced Optical Microscopy Centre, Biomedical Research Institute, Agoralaan C (BIOMED), Hasselt University, B-3590 Diepenbeek, Belgium

[4]Lead Contact

*Correspondence: jelle.hendrix@uhasselt.be (J.H.), tassos.economou@kuleuven.be (A.E.)

https://doi.org/10.1016/j.str.2018.10.006

SUMMARY

SecA converts ATP energy to protein translocation work. Together with the membrane-embedded SecY channel it forms the bacterial protein translocase. How secretory proteins bind to SecA and drive conformational cascades to promote their secretion remains unknown. To address this, we focus on the preprotein binding domain (PBD) of SecA. PBD crystalizes in three distinct states, swiveling around its narrow stem. Here, we examined whether PBD displays intrinsic dynamics in solution using single-molecule Förster resonance energy transfer (smFRET). Unique cysteinyl pairs on PBD and apposed domains were labeled with donor/acceptor dyes. Derivatives were analyzed using pulsed interleaved excitation and multi-parameter fluorescence detection. The PBD undergoes significant rotational motions, occupying at least three distinct states in dimeric and four in monomeric soluble SecA. Nucleotides do not affect smFRET-detectable PBD dynamics. These findings lay the foundations for single-molecule dissection of translocase mechanics and suggest models for possible PBD involvement during catalysis.

INTRODUCTION

Protein export is an essential and ubiquitous process that affects >30% of the proteome (Rapoport, 2007; Tsirigotaki et al., 2017). Many bacterial pathogenicity factors are secreted proteins and some diseases result from faulty protein targeting. Despite progress, the molecular mechanism of this fundamental process is still unclear.

Bacteria such as *Escherichia coli* are ideal models to study protein secretion. All proteins necessary for translocation through the main Sec pathway are known, as are their structures, and functional assays are available (Tsirigotaki et al., 2017). The 505 secretory preproteins of *E. coli* are sorted from cytoplasmic proteins and targeted post-translationally using signals on their N-terminal peptides and mature domains and chaperones (Chatzi et al., 2017; Gelis et al., 2007; Gouridis et al., 2009; Tsirigotaki et al., 2017). Preproteins are recognized by the protein translocase comprising the dimeric peripheral SecA ATPase bound to the SecYEG membrane-embedded protein-conducting channel and trigger their energy-dependent transport (Tsirigotaki et al., 2017).

SecA undergoes dimer-to-monomer equilibria on the ribosome (Huber et al., 2011), cytoplasm, and SecYEG (Gouridis et al., 2013). Its intracellular concentration is ~5.7–8.2 μM (Akita et al., 1991; Woodbury et al., 2002), and it dimerizes with multiple arrangements of sliding protomers in equilibrium (Gouridis et al., 2013), with a dissociation constant of ~1 nM (Kusters et al., 2011; Wowor et al., 2011).

The SecA protomer comprises four domains (Figure 1) (Sardis and Economou, 2010): the nucleotide binding domain (NBD), intramolecular regulator of the ATPase2 (IRA2 or NBD2), preprotein binding domain (PBD), and the C domain, containing the flexible helical sub-structure termed Wing domain (WD). NBD and IRA2 form an RNA helicase DEAD motor, and sandwich nucleotides. The PBD and the C domain recognize preproteins and SecYEG (Chatzi et al., 2017; Gelis et al., 2007; Zimmer and Rapoport, 2009). In various crystal structures, the PDB swivels by ~60°, giving rise to three states: closed, open, and wide open (Figure 1) (Sardis and Economou, 2010). This motion forms an apparent PBD-IRA2 clamp (Figure 1) that is not required for initial preprotein docking to SecA (Chatzi et al., 2017) but that may accommodate translocating chains (Bauer and Rapoport, 2009). PBD motions may contribute to translocation initiation (Gold et al., 2013), but whether they occur outside crystal lattices and how they might participate in translocase catalysis remain unknown.

To better understand protein translocase mechanics a deeper, quantitative understanding is needed of SecA conformational changes and dynamics, typically offered by state-of-the-art biophysical approaches. A notable ensemble approach is hydrogen-deuterium exchange mass spectrometry (HDX-MS) (Sardis et al., 2017; Tsirigotaki et al., 2018). At the single-molecule level, Förster resonance energy transfer (FRET), the near-field (1–10 nm) radiation-less transfer of energy from an excited

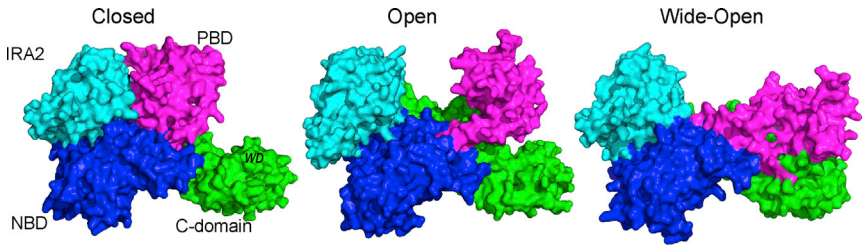

Figure 1. Domain Organization of SecA and PBD States in Solved X-ray Structures

E. coli SecA structures: the indicated conformational PBD states motions (closed, open, wide-open), modeled (Chatzi et al., 2017) after the *E. coli*, open model (PDB: 2FSF, open), seen by NMR and based on crystal structures, available on PDB (closed: PDB: 3DIN; *Thermotoga maritima*. Wide open: PDB: 1M6N; *Bacillus subtilis*). SecYEG would bind at the back of each structure in the translocase complex (Figure S7).

donor fluorophore to an excitable acceptor fluorophore, is particularly powerful (Förster, 1946; Zander et al., 1996). Single-molecule Förster resonance energy transfer (smFRET) monitors intramolecular (conformational rearrangements/domain motions) or intermolecular (association/dissociation) dynamic processes in real time. Thus distinct conformational states, commonly lost in ensemble measurements, can be identified (Ha and Tinnefeld, 2012; Roy et al., 2008) and their physical distances derived from the measured Förster resonance energy transfer (FRET) quantum efficiency (*E*) between the probes (Hellenkamp et al., 2018; Kapanidis et al., 2004; Lee et al., 2005; Vandenberk et al., 2018). In solution smFRET, fluorescent molecules diffuse freely through the confocal volume of a microscope (Figures 2A and S1A) and their fluorescent bursts (i.e., the number of photons they emit during the time they stay in focus) are measured (Eggeling et al., 2001; Kellner et al., 2014; Zander et al., 1996). In such analyses, the donor and acceptor fluorophores can be excited in an alternating fashion on the nanosecond timescale (referred to as pulsed interleaved excitation [PIE]) and registered via multi-parameter fluorescence detection (MFD) (Figures 2A and S1A), with each photon being detected by time-correlated single-photon counting (Figure S1A) (Hendrix and Lamb, 2013; Kudryavtsev et al., 2012; Müller et al., 2005). This yields a wealth of information on both the FRET donor and acceptor, including fluorescence intensity, lifetime, anisotropy, and color (Figure 2A). smFRET can detect a broad range of timescales in protein folding/conformational rearrangements (nanoseconds to minutes). These include dye rotation (nanoseconds); unfolded state dynamics (nanoseconds to microseconds); folding/rearrangements (microseconds to seconds), which depend on ultra-fast motions of structured protein parts (picoseconds to microseconds); fast whole-domain motions (microseconds to milliseconds); and misfolding/oligomerization (seconds to minutes or hours) (Schuler and Hofmann, 2013). smFRET, combined with MFD-PIE and proper time-resolved analysis, discriminates the intrinsic protein dynamics that are of biological interest from the chemical properties of the labels and the artifacts and photophysical dynamics that need to be excluded (Cotlet et al., 2005; Hofkens et al., 2003; Vandenberk et al., 2018; Vosch et al., 2003).

Here we present the first smFRET/MFD-PIE-based pipeline to study the conformational dynamics of the PBD domain of SecA on a timescale of 0.1–10 ms. Residues, ideally located for FRET, were mutated into unique cysteinyl (cys) pairs and tested for functionality *in vivo*. Derivative proteins were labeled and tested for functionality *in vitro*. Finally, physical distances of PBD motions were determined by photon distribution analysis (PDA) (Antonik et al., 2006; Kalinin et al., 2008).

Using smFRET we determined that the PBD displays intrinsic domain swiveling in solution. It samples at least three conformational states that approximate those in crystal lattices but vary in their abundance. Dimer-to-monomer transition not only shifts the equilibrium between the observed PBD states and the physical positioning of PBD but also gives rise to a fourth state. We hypothesize that the intrinsic mobility of PBD allows (1) binding of hundreds of dissimilar, non-folded preproteins; (2) mechanical motions in the SecY-bound state to promote translocation. In the functionally quiescent soluble dimeric and the monomeric SecA, these PBD motions are uncoupled from nucleotide binding to the ATPase motor. These data set the foundations for future quantitative dissection of SecA and translocase dynamics in the presence of all the reaction ligands during ongoing translocation.

RESULTS

A Five-Step Pipeline for smFRET Analysis of SecA

The conformational dynamics of the PBD domain of SecA were investigated using a five-step pipeline (Figure S2A): (1) selection of optimal residues for placing donor/acceptor dye pairs; (2) generation of mutants, testing of their *in vivo* function, gene overexpression, and protein purification; (3) optimization of labeling with fluorescent probes; (4) smFRET measurements, data analysis, and statistical treatment; and (5) derivations of physical distances of PBD motions.

Selection of SecA Residues and Cys Mutagenesis

For residue-specific labeling via maleimide-modified dyes reacting with thiol groups of cys residues (Figure S1C), we used the fully functional SecA(Cys$^-$) (Chatzi et al., 2017; Sardis et al., 2017). The *secA*(cys$^-$) gene derivatives with specific cysteine pairs were generated. Based on six selection criteria and the anticipated changes in FRET according to FRET-restrained positioning and screening (see STAR Methods) (Figure S1D and Table S1), 31 possible FRET pairs were identified (Table S2). Target residues were mutagenized (STAR Methods; Tables S3 and S4). All but one of the mutated genes were shown by genetic complementation to restore growth to strain BL21.19, which carries a chromosomal thermosensitive *secA* (Karamanou et al., 1999). Therefore, cys mutagenesis did not affect SecA functionality. Next, mutated SecA derivatives were purified to homogeneity (Gouridis et al., 2013; Papanikolau et al., 2007) in the presence of high concentrations of a dithiol reducing agent (e.g., dithiothreitol [DTT]), to maintain optimal labeling (Figure S2E) and stored for up to 2 months (50% volume per volume glycerol, −20°C) (Figure S2F). Some derivatives displayed altered dimerization equilibria and were not studied further (Figures S2A and S2B).

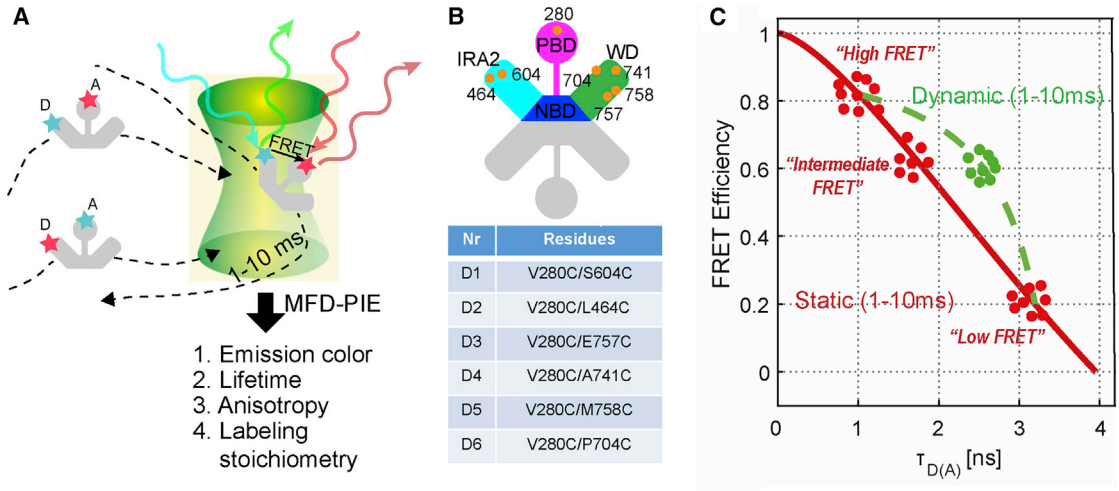

Nr	Residues
D1	V280C/S604C
D2	V280C/L464C
D3	V280C/E757C
D4	V280C/A741C
D5	V280C/M758C
D6	V280C/P704C

Figure 2. Principles of smFRET Using MFD-PIE

(A) Illustration of burst-wise smFRET using MFD-PIE (left; Figures S1A and S1B) with some of the information obtained from a single burst measurement and potential derived information relating to protein structure (right).

(B) SecA derivatives (D1–6) selected (Figure S2A) to optimally report on potential PBD motions toward the IRA2 or the WD domains. Gray cartoon: the second unlabeled protomer of the dimer.

(C) Schematic representation of anticipated MFD-PIE results plotted on a 2D graph showing measurements distributed in the cases of hypothetical static and dynamic FRET models. A protein with three conformational states, closed (high FRET), intermediate, and one open (low FRET), results in three donor burst-averaged fluorescence lifetimes, τ_1, τ_2, and τ_3 (red dot clouds), respectively. In the case of a slow interconversion between states (i.e., >10 ms), data clouds are positioned on the static FRET line (solid red) and τ_1, τ_2, and τ_3 can be determined. Faster interconversions result in averaged data clouds along the dynamic FRET line (dashed green line), and only a fluorescence-weighted average lifetime can be observed (Gansen et al., 2009; Kudryavtsev et al., 2012).

Labeling of SecA Double-Cys Derivatives

DTT was removed and SecAs were labeled using two different donor (D)/acceptor (A) maleimide-attached dye pairs under pH 6.5–7.5 (Figure S2C) (Brewer and Riehm, 1967): ATTO488/ATTO647N and ATTO488/Alexa 647. Measurable nonspecific labeling of SecA(Cys^-) occurred with ATTO647N but not with Alexa 647 or ATTO488 (Figure S2D). Therefore, ATTO488/Alexa 647 were used thereafter. Since both dyes are added simultaneously, mixed labeled populations were obtained containing both hetero-labeled (D and A or A and D on either one of the two cys residues; both usable; Figure 2A) and homo-labeled (D or A only). However, PIE allows the unwanted homo-labeled molecules to be removed during data analysis (Kudryavtsev et al., 2012). A hetero-labeling efficiency of 40%–60% was typically obtained.

Labeled SecAs were re-purified by size-exclusion chromatography, collecting only the narrowest, highly homogeneous chromatographic peaks, and removing free dye and protein aggregates. Purified, labeled SecAs were found to be fully functional using an established *in vitro* assay that measures their ability to have their ATPase activity stimulated by secretory preproteins in the presence of membrane vesicles (Gouridis et al., 2010).

Accurate Measurement of Physical Positioning of PBD States in Soluble SecA

To report on all the possible anticipated PBD motions against either WD of the C domain or the IRA2 domain, we used thereafter six of the double-cys SecA derivatives, which satisfied the previous preparative steps (D1–6; Figure 2B). To directly compare distances in the six derivatives, they shared one of the two cys residues (V280C on PBD) (Figure 2B).

Accurate physical distances of PBD motions were derived using PDA (Antonik et al., 2006; Kalinin et al., 2008). For PDA to provide reliable structural information, the donor and acceptor dye spectroscopic properties when attached to the molecule of interest need to be verified. Considerable quenching of the dye's fluorescence, independently of FRET, results in a lower lifetime and quantum yield, which complicates further analysis. Anisotropy values that are too high could reflect partial sticking of the dyes (which are overall negatively charged) on positively charged neighboring protein surfaces. This in turn causes unpredictable shifts in FRET efficiency, or even in the appearance of nonsense FRET states, and renders the derived distances and distance distributions inaccurate. Therefore, we first focused our analysis on the donor dye for proteins that were labeled only by the donor (to be able to study the dye in the absence of FRET) or on the acceptor dye for double-labeled proteins. When plotted in a r_D-τ_D or r_A-τ_A 2D histogram (with the fluorescence lifetime of the FRET donor, τ_D, that of the acceptor, τ_A, the steady-state anisotropy of the FRET donor, r_D, and of the acceptor, r_A), the data points are preferentially localized in one main fluorescence lifetime and anisotropy population, with the fluorescence lifetime preferentially close to that of the free dye, and the anisotropy preferentially low. On the other hand, if the dyes exhibit heterogeneous lifetimes or anisotropy values, then care must be taken in further analysis.

For the six SecA derivatives that were analyzed, we next investigated the donor dye of donor-only labeled molecules and the acceptor dye of double-labeled molecules. D1, D2, and D3 displayed single populations for both lifetime and anisotropy and the exact expected lifetime of the donor dye (4.0 ns; ATTO-TEC) (Figures S3B–S3D). D5 also displayed single populations

overall; however, a minor second anisotropy population slightly appeared for the donor (Figure S3F).

On the other hand, derivative D4 displayed at least two anisotropy populations of the donor with the high anisotropy state being higher populated (Figure S3E). D4 was not used further. Derivative D6 shows a major (4.0 ns) and minor (2.5 ns) lifetime distribution of the donor-only population, likely reflecting dye-protein interactions (data not shown). Therefore, D6 was not used further.

Taken together, our analysis of protein-attached dye behavior allowed us to retain only those double-cys mutants that ensured deriving accurate structural information from PDA analysis (see below).

Optimization of Quantitative smFRET Measurements, Data Processing, and Analysis

Next, we analyzed the fluorescently hetero-labeled SecAs by MFD-PIE to detect smFRET bursts and deduce conformational behavior. Getting enough bursts from doubly hetero-labeled SecAs, in the shortest possible time yields high quality data due to the collection of several thousand single-molecule samples and minimizes potential loss of SecA functionality. Condition optimization included BSA-coated coverslips and soluble agents such as free BSA or Trolox to prevent nonspecific protein absorption and photo-bleaching) (Figure S2G) (Aitken et al., 2008; Rasnik et al., 2006; Vandenberk et al., 2018; Vogelsang et al., 2008).

Primary experimental values from thousands of bursts are graphed in 2D plots of FRET efficiency (Figure 2C; y axis) against the fluorescence lifetime of the donor in the presence of the acceptor ($\tau_{D(A)}$; x axis). In these plots, the burst data points are distributed in one or more "clouds" along a curved diagonal (Figure 2C) (STAR Methods: "Burst-wise fluorescence lifetime"). The curved diagonal intersects the x axis at the lifetime of the donor-only population and the y axis at unity.

When FRET states do not interconvert during the single-molecule observation time (0.1–10 ms), the FRET of the molecules is said to be "static" and photon bursts from the protein's fluorescent probes will have values that fall tightly on the diagonal, commonly referred to as the 'static FRET line' (red). If more than one "cloud" of data co-exist on the static FRET line for the same protein, or if the clouds are poly-dispersed, the protein molecules as they travel through the confocal volume exist in and retain multiple conformational states. This "solution" analysis can define the specific conformational states sampled and how well they are represented in the whole population.

Burst values that deviate to the right of the diagonal (Figure 2C, green dots) would indicate that the two fluorescent probes, and hence the SecA domains on which they are carried, display conformational dynamics that occur during the timescale of the measurement, i.e. while the protein is diffusing through the focus of the laser (0.1–10 ms).

Analysis of PBD Motions in Soluble SecA by smFRET

We next proceeded to analyzing smFRET-derived PBD motions in dimeric SecA derivatives D1, D2, D3 and D5 by mixing ~100–200 pM of fluorescently labeled with 100 nM of unlabeled SecA, 100-fold over the dimerization K_d (Figures 3 and S4, left) (Kusters et al., 2011). This allows analyzing smFRET events from a single hetero-labeled SecA protomer but within the context of the physiological SecA dimer (Figures 3A and 3B, left, cartoon). Primary experimental values were graphed in 2D plots of FRET efficiency against the fluorescence lifetime of the donor (as in Figures 3 and S4, left), of the many parameters were obtained by MFD-PIE detection, six are shown for a representative SecA derivative (Figure S3A). In all cases, results reported in this study are consistent with "static FRET" behavior for PBD motions (Figure 2C, red).

The PBD of derivative D1 that probes a potential PBD to IRA2 motion, showed a high FRET state in one-third of the molecules (Figure 3A). The structural interpretation is, therefore, that in these molecules that diffused through the confocal volume, their PBD is positioned within ~4 nm of IRA2 (state 1). However, a discernible number of bursts, display lower (state 2; ~50%) or much lower (state 3; ~10%) FRET efficiencies and, therefore, several of these SecA molecules have their PBD positioned away from IRA2 (6 or more nm; state 2 and 3). These results are corroborated and strengthened by the analysis of D2 that also probes the PBD to IRA2 motion (Figure S4A, left). They demonstrate that in a given population of soluble SecA, the PBD samples multiple conformational states.

In D3, that probes the PBD to WD motion, the PBD occupies low and medium FRET states for most of the bursts measured (Figure 3B, left). This implies that in most of the molecules diffusing through the confocal volume, PBD is positioned away from WD residues in this pair. D5 (Figure S4C, left) also probes the same inter-domain interaction. D5 showed a predominantly low and a minor-high FRET state that would be compatible with the FRET pair in some molecules having a "closed" PBD-WD interface. Because of the distributions in two distinct clouds, D5 also supports the existence of at least two stable PBD states.

Accurate Measurement of Physical Positioning of PBD States in Soluble SecA

The multiple probe pairs allow an approximate triangulation of the positions of PBD in SecA using FRET-derived structural distances by visually estimating E from the 2D plots (Figure S4E, Left). This approximation is more accurate for samples that exhibit small, tightly distributed FRET populations and not for the smFRET data of the PBD showing broadly distributed states for some derivatives. FRET-competent states may be too close to be distinguished by eye and thus accurate physical distances of PBD motions were determined by PDA (Antonik et al., 2006; Kalinin et al., 2008).

Conformational dynamics in the 0.1–10 ms timescale (Figure 2C, green) can be detected by cutting the burst data into time windows of specified length. This 'time window analysis' did not reveal clear differences between the FRET histograms for D1, D2, D3 and D5 (Figure S5 and Data S2), indicating the PBD displays no conformational dynamics in the 0.1–10 ms timescale. In other words, PBD moves from one of its states to the other more slowly than 10 ms. Therefore, a PDA model incorporating different FRET states was fitted to the data, with each state assuming a Gaussian distance distribution (Kalinin et al., 2008, 2012; Talavera et al., 2018) (Figures 3A, 3B, right, S6A, and S6B). This analysis revealed that taken collectively, D1 (Figure 3A), D2 (Figure S6A, right), D3

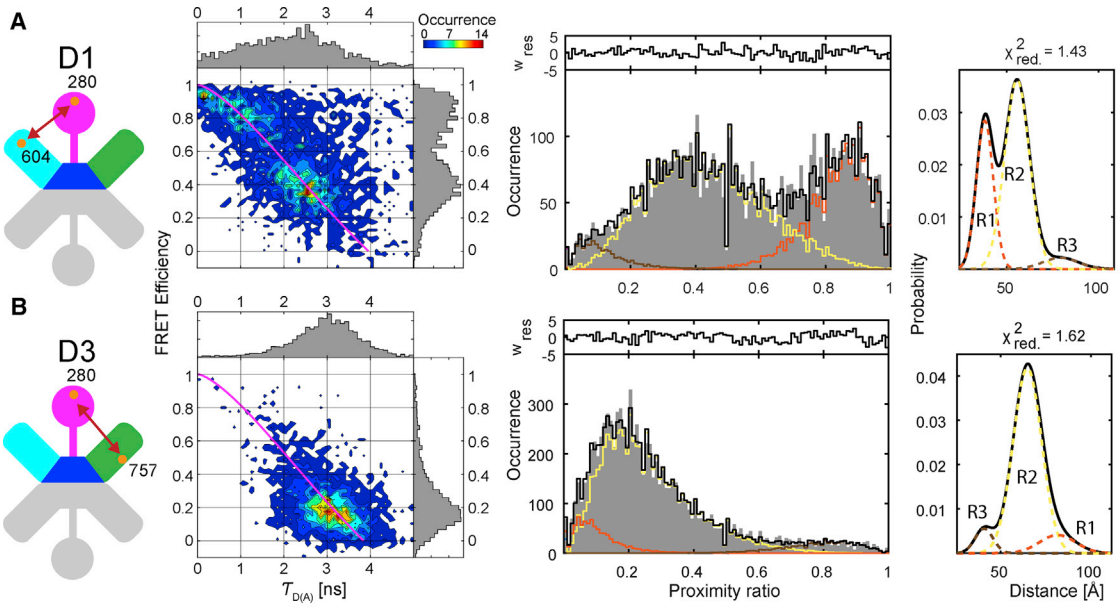

C

	state 1				state 2				state 3			
SecA derivative	A_1 (%)	σ_{A_1}	R_1 (Å)	σ_{R_1}	A_2 (%)	σ_{A_2}	R_2 (Å)	σ_{R_2}	A_3 (%)	σ_{A_3}	R_3 (Å)	σ_{R_3}
D1	38	7	38	3	56	9	56	3	6	1	79	3
D2	49	2	39	3	40	1	50	3	11	2	70	3
D3	9	2	82	8	82	1	65	2	9	2	41	3
D5	5	1	86	4	87	2	62	3	8	2	39	2

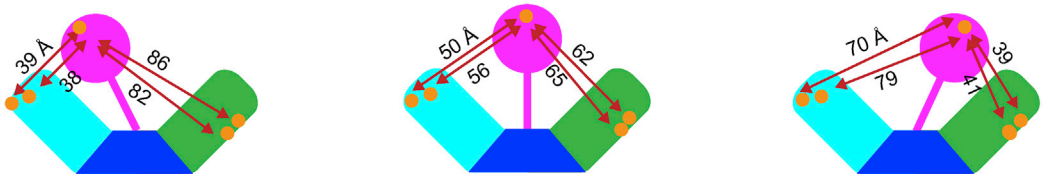

Figure 3. smFRET-Derived PBD Structural States in Dimeric SecA

(A and B) Analysis of PBD conformational dynamics studied within the context of dimeric SecA. Left, cartoons of the derivatives. Middle, 3,000–4,000 individual bursts each from the six indicated derivatives were plotted on 2D plots of E versus $\tau_{D(A)}$. This lifetime ($\tau_{D(A)}$) is the burst-averaged fluorescence-weighted lifetime of the donor in presence of the acceptor, integrated over the collected photons per burst. Contour plots display 2D histograms of molecule counts (red = high, blue = low counts). The 1D bar charts are projections of the 2D histograms on the respective axes. Static FRET lines (red) were calculated with Equation 6. Right, PDA of D1 (A) and D3 (B) for the dimeric condition in a global fit (STAR Methods and Figure S6). Uncorrected proximity ratio histograms (gray bars). Black stairs, total PDA model; colored dashed stairs, subpopulations. w_{res} = weighted residuals (top graph). Corresponding distance distribution plots illustrating the intricate relation of distance and FRET distribution width. Black solid line, total model; colored dashed lines, sub-states.

(C) smFRET-determined PBD states in soluble dimeric SecA summarized in a table with the fraction A (%) of each population distribution and the derived distances (Å) after PDA analysis in three possible states. For additional data on D2 and D5, see Figures S4 and S6. Errors in the table were calculated as defined in the STAR Methods section.

(Figure 3B) and D5 (Figure S6B, right) support the existence of the same three clearly defined PBD states (1, 2 and 3) (Figure 3C). PBD is either almost equidistant from IRA2 and WD (state 2, Figure 3C, bottom) or moves close to IRA2 (state 1) or to WD (state 3). The fraction of molecules that occupy these states is distinct: more than half populate state 2, followed by state 1 and 3.

In summary, D1, D2, D3, and D5 were analyzed globally using PDA. PBD occupies three distinct states in solution, with state 2 being the most populated.

Dimer to Monomer Transition Affects PBD Motions

During catalysis, SecA undergoes dimer-to-monomer transitions (Gouridis et al., 2013; Singh et al., 2014). To investigate if

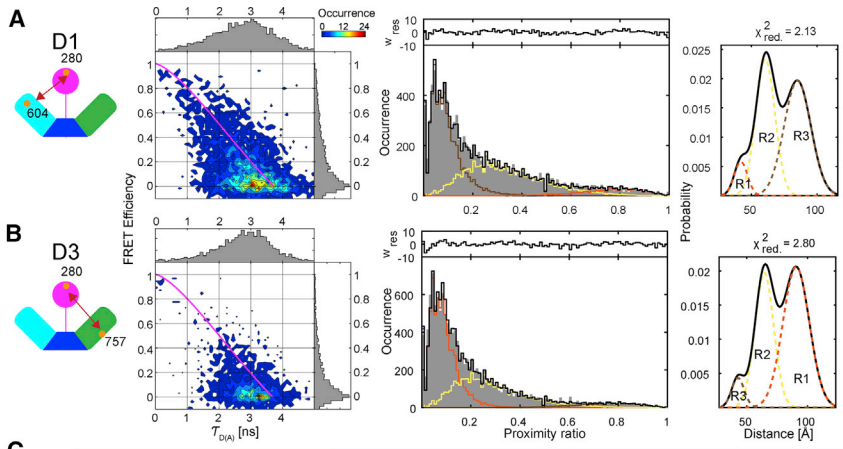

C

	state 1				state 2				state 2A				state 3			
SecA derivative	A_1 (%)	σ_{A_1}	R_1 (Å)	σ_{R_1}	A_2 (%)	σ_{A_2}	R_2 (Å)	σ_{R_2}	A_{2A} (%)	$\sigma_{A_{2A}}$	R_{2A} (Å)	$\sigma_{R_{2A}}$	A_3 (%)	σ_{A_3}	R_3 (Å)	σ_{R_3}
D1	6	2	42	2	37	6	61	3	~51	8	85	3	~6	8	85	3
D2	7	4	40	3	49	2	58	4	~38	6	81	3	~6	6	81	3
D3	~7	5	91	5	44	5	65	3	~43	5	91	5	6	1	43	5
D5	~7	4	90	3	37	3	66	3	~52	4	90	3	4	1	44	5

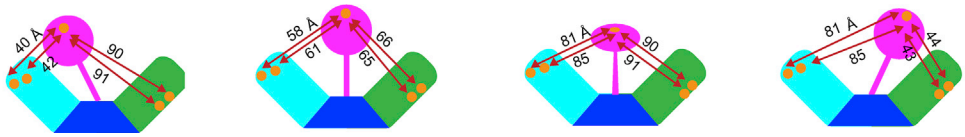

Figure 4. smFRET-Derived PBD States in Monomeric SecA

(A and B) Analysis of PBD dynamic conformational behavior when studied within the context of monomeric SecA (as in Figures 3A and 3B). (C) Summarized PBD physical motions derived from PDA in monomeric SecA (as in Figure 3C).

monomerization affects PBD conformations and dynamics, we examined the four fluorescently labeled SecA derivatives at concentrations of 100–200 pM, which, based on the determined K_d of ~1 nM (Kusters et al., 2011), should push the equilibrium mainly to monomers (Figure 4, left and S4, right). PDA analysis of monomeric D1, D2, D3, and D5 (Figures 4A, 4B, S6A, and S6B) was carried out to obtain accurate measurements of the positioning of PBD states.

Monomeric D1 (Figure 4A, left), which probes the PBD to IRA2 inter-domain motion, exists in three states with largely similar distances to those of dimeric SecA, and a fourth state, termed 2A, protruding away from the main protein body, also became apparent (Figures 4A and 4C). The occupancy ratio between the states showed significant changes compared with that in the dimer. PBD in the majority of the monomeric molecules now occupy states 2 and 2A (>85%) at the expense of state 1. State 3 remains poorly populated (Figure 4C). The PBD of monomeric D2, which also probes the PBD to IRA2 inter-domain motion (Figure S4A, right), yielded shifts like those of D1 (Figure 4C). These data demonstrated that PDB stays away from both IRA2 and WD in most of the monomeric SecA molecules that diffused through the confocal volume, while half of the state 2 PBDs swivel away from the protein body.

In D3 and D5 (Figures 4B, S4B, and S4C, right) that probe the PBD to WD motion, the PBD of the monomer samples low-FRET states for most of the individual bursts measured. Therefore, the PBD is positioned far away from its respective WD residue pairs; >8 nm in most of the molecules of both derivatives. D3 and D5 displayed four distinct PBD states after PDA with similar ratios of those states but with different distances compared with those of monomeric D1 and D2 (Figure 3C).

To further corroborate the data obtained above at the concentrations of presumed SecA monomerization and to exclude contributions from surviving dimeric molecules, we used a genetically constructed monomer derivative, mSecA, which displays a 10^5-fold loss in its dimerization K_d (~133 μM) but becomes dimeric and fully functional at high concentrations (Gouridis et al., 2013). We constructed mSecA variants with the four cys-pair derivatives and determined their smFRET profiles. These profiles were highly comparable with those of kinetic monomers generated after dilution (Figure S3G; D1 shown as a representative example).

The detected differences between dimeric and monomeric states allowed determination of the K_d of this transition. Unlabeled SecA D1 was titrated into reactions containing 200 pM fluorescently labeled D1 (kinetic monomer conditions) (Data S1A–S1J), changes to the three observed PBD states

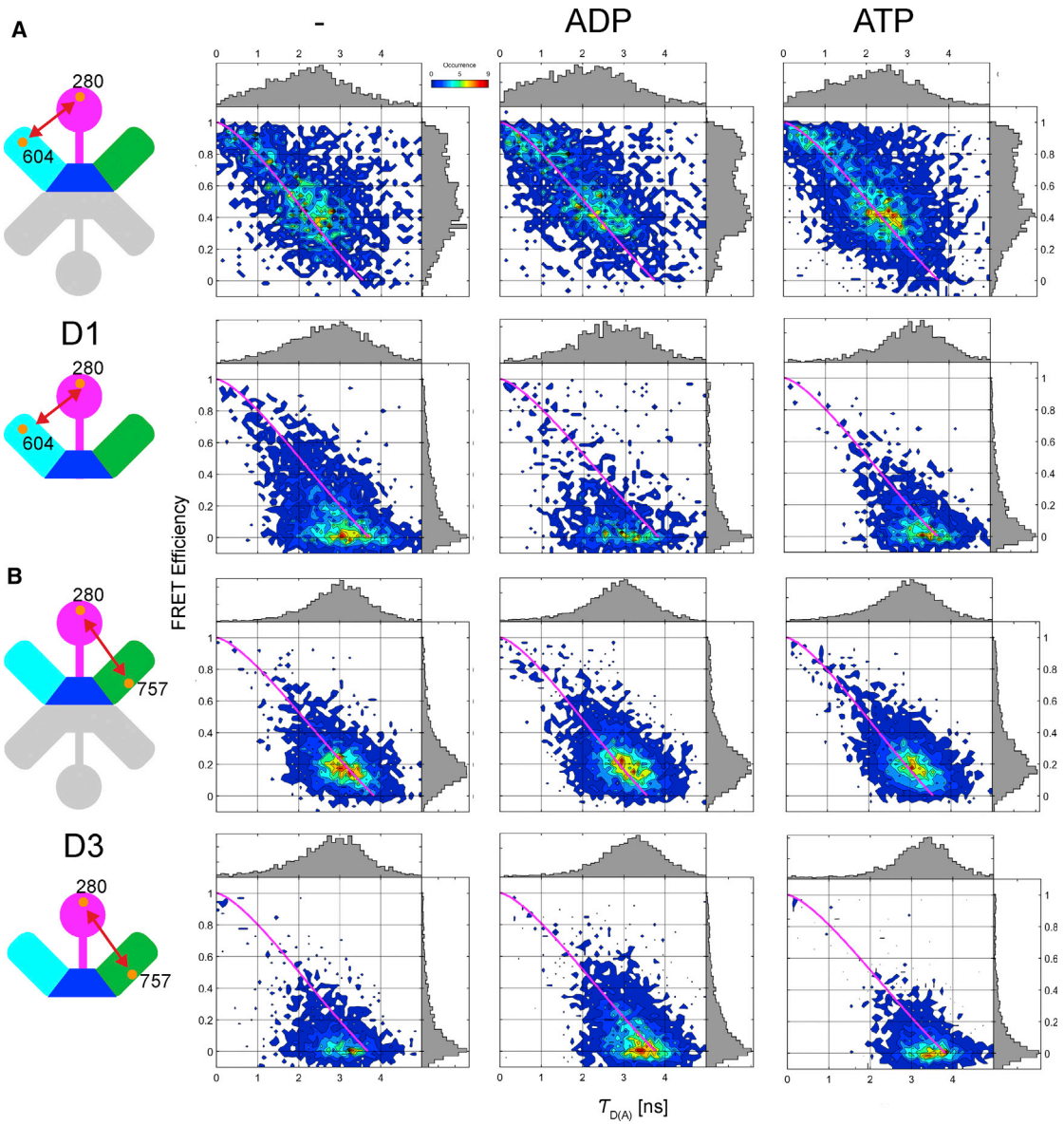

Figure 5. ADP-Independent PBD Motions in Soluble SecA

Nucleotides have limited effect on PBD motions in soluble SecA. Effect of ADP and ATP on dimeric (above) and monomeric (below) (K_d see Data S1) SecA for D1 (A) and D3 (B). Left, dimeric SecA: 200 pM labeled SecA with addition of 100 nM unlabeled SecA. Middle, Dimeric SecA with ADP: 200 pM labeled SecA with addition of 100 nM unlabeled SecA, 10 μM ADP, and 50 μM $MgCl_2$. Right, dimeric SecA with ATP: 200 pM labeled SecA with addition of 100 nM unlabeled SecA, 10 μM ATP, and 50 μM $MgCl_2$.

(Figure 3) were monitored, and a sigmoid was fitted to the data. A K_d of 2.2 nM and 3.0 nM for state 3 and 1, respectively were derived (Data S1K), close to the one previously obtained (0.74 nM; Kusters et al., 2011). Additionally, burst-wise fluorescence correlation of every single-molecule event (see STAR Methods) revealed a significant difference in diffusion coefficient between the monomeric and dimeric state of D1, indicative of a hydrodynamic property change of the protein (Data S1L).

Taken together, SecA monomerization causes significant conformational differences to the PBD relative to those in the dimer state, both in terms of number and the fraction of the population that occupies the conformational states.

Nucleotides Have Only a Minor Effect on PBD Dynamics

SecA in solution binds ATP, rapidly converts it to ADP, and acquires the quiescent, thermally stabilized state (Keramisanou et al., 2006; Sianidis et al., 2001). However, addition of ADP to dimeric SecA leads to no changes in the FRET states of the PBD (Figures 5A and 5B). The same is seen with ATP (Figures 5A and 5B). Similar effects were seen with the kinetic SecA monomer (Figure 5B).

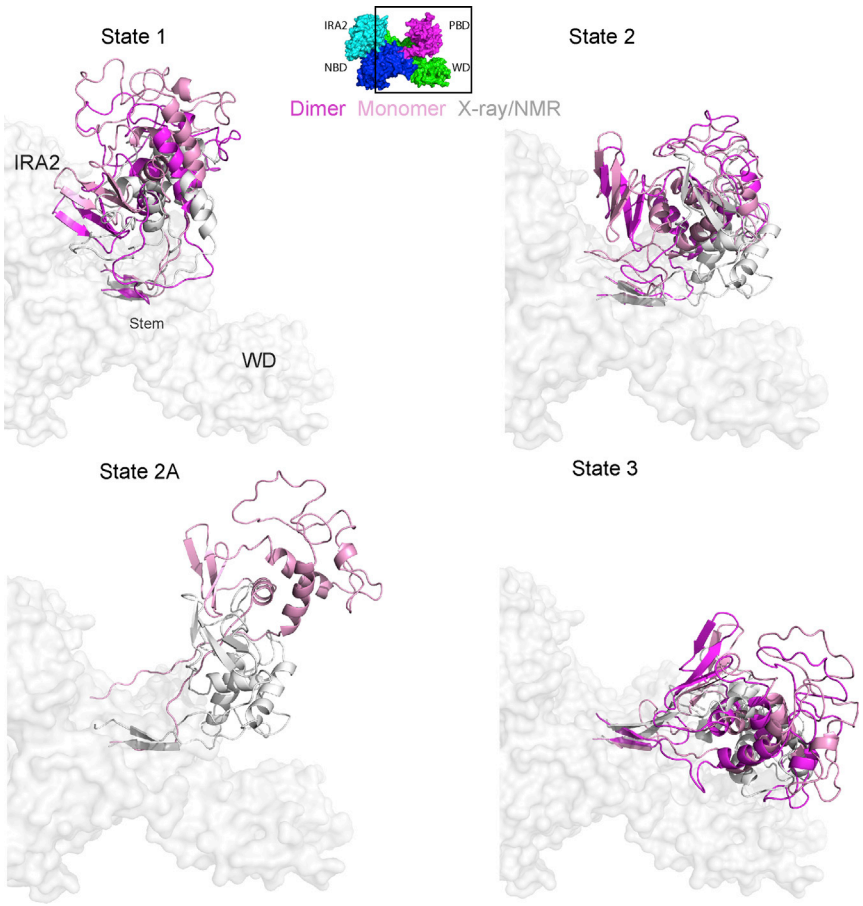

Figure 6. Visualization Models of the smFRET-Derived PBD States of SecA

Zoomed-in views (defined by the square in the four-colored SecA surface structure; top) of the four different states of the PBD (ribbon; colored as indicated) modeled according to the smFRET-derived distance restraints (Table S5). The modeled PBDs are overlaid to those of the already solved SecA structures (dark gray: PDB: 3DIN in state 1, closed; PDB: 2VDA in state 2, open and state 4; PDB: 1M6N in state 3, wide open). The body of SecA, including parts of IRA2 and WD, is shown as a white surface and the stem antiparallel β strands are indicated.

These data suggest that, in the quiescent state of soluble SecA, nucleotide interactions in the ATPase motor of SecA are not transmitted to the PBD or cannot be detected in our assay.

Visualizing the Different PBD States in Soluble SecA by Rigid Body Modeling

As it undergoes the motions detected here, the PBD does not lose internal secondary structure as determined by HDX-MS (Krisnamurthy et al., unpublished data). Therefore, it largely undergoes rigid body rotations. To visualize these complex motions in 3D space in SecA in solution, we rotated the PBD as a rigid body around its stem, using the beginning of the stem as a fixed point. In the absence of any currently available information on SecA structural dynamics, we made the simple assumption that, as seen in crystal structures, no additional large motions occur in the three other domains of SecA. Thus, while maintaining the rest of SecA as a rigid body, we used the FRET-derived distances as restraints (Figures 3C and 4C). The three smFRET-derived PBD states of dimeric SecA differ slightly (e.g., state 1 versus the closed state; Figure 6, magenta) or more substantially (e.g., state 2 versus the open state), from the three PBD states seen in crystal structures (gray).

The four states calculated by smFRET for monomeric SecA (Figure 4C) were also visualized (Figure 6, pink). States 1–3 are closer to the ones seen in the dimer, while state 2A is clearly distinct and has not been seen before in X-ray-derived structures. The PBD of state 2A relates to the crystallographic open state and the smFRET-derived state 2 of the dimer but projects further away from the rest of the protein and is leaning closer to the IRA2. Additional restraints combined with dynamic modeling of the structure will be required to trace these complex motions during catalysis.

DISCUSSION

We present the first, to our knowledge, complete pipeline for generating solution-smFRET-compatible, hetero-labeled, fully functional SecA and measuring its conformational domain dynamics. This effort aims to take translocase studies beyond X-ray crystallography or nuclear magnetic resonance (NMR), focusing on structural and conformational dynamics analyzed under native conditions.

Here, we focused on the conformational domain dynamics of the PBD of SecA. This domain was an attractive target for multiple reasons: firstly, PBD binds signal peptides and, together with the C domain, mature domains (Chatzi et al., 2017; Gelis et al., 2007). Preprotein clients are likely to affect PBD dynamics and perhaps even exploit them to convert ATP cycling to translocation-related work. Secondly, the PBD occupies different states in crystal structures. Such PBD motions may be coupled to mechanical work, although, currently, there is no direct structural evidence for this. Prior to this study, it was unknown if and to what extent PBD motions might occur in SecA in solution. Finally, seen from a technical, smFRET perspective, if PBD motions did indeed occur, they would provide distance changes that could be appropriately probed by smFRET.

Using smFRET we determined that the PBD of soluble dimeric SecA samples at least two major states (state 2 of ~40%–50% and state 1 of 40%–50% of the molecules) and a minor state (state 3; 5%–10%) (Figures 3C and 6). The distances of these states are similar to the ones in crystal structures, yet deviate from them by 2%–15%, suggesting that the crystal lattices selected/stabilized slightly different PBD states (Figure 6).

Site-directed spin labeling and NMR-detected paramagnetic relaxation enhancement analysis, which previously probed PBD to WD motions, suggested the state 2 (open) and state 3

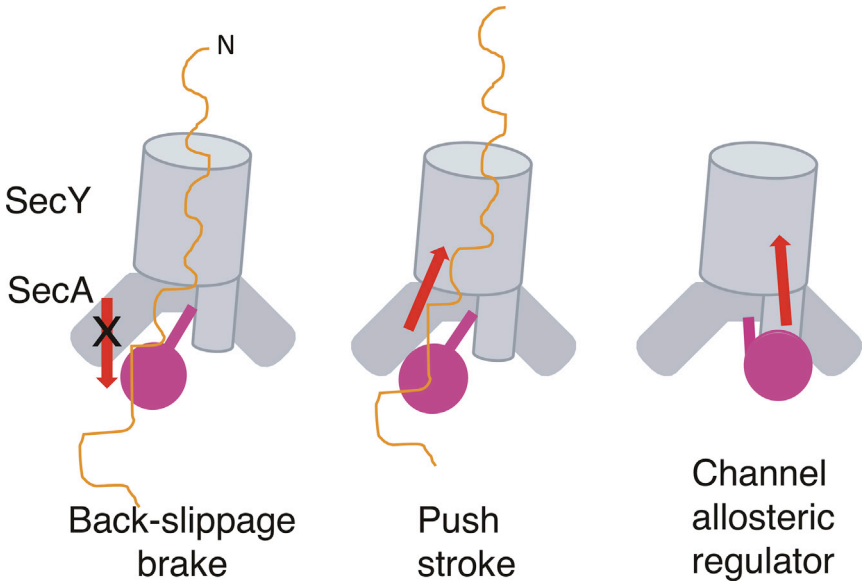

Figure 7. Hypothetical Models of PBD Function during Translocation

Three hypothetical models of how PBD swiveling (magenta) might mechanistically contribute to preprotein (orange) translocation through SecYEG (see also Figure S7).

(wide open) may be occupied by 90% and 10% of the molecules, respectively (Gelis et al., 2007). Single-molecule dissection now reveals that the intrinsic dynamics of PBD are more complex, with the 90% population being split between states 2 and 1.

PBD swiveling is significantly affected when SecA monomerizes (Figure 4). Four distinct PBD populations are discernible but both the measured distances and distribution of molecules between them changed compared with those of the dimer. Many molecules also display a new state 2A, comparable with state 2 but with the PBD moved further away from the body of the protein. Therefore, PBD not only displays remarkable rotational dynamics but also the states that it occupies are structurally distinct. Occupancy of these apparent stable energetic minima are influenced by the quaternary state of SecA. These states interconvert slowly in tens of milliseconds, characteristic of whole-domain motions (Schuler and Hofmann, 2013). How they interconvert, with which rate constants, in which order, and what their lifetimes are will require future prolonged smFRET kinetic measurements of immobilized molecules (Roy et al., 2008). Diffusion measurements using our MFD-PIE setup cannot define these slow rate constants (<0.1 ms^{-1}). The 2D plots also hint at the presence of rare kinetic exchanges that are faster than the burst duration. The latter could be investigated in more detail by using approaches like filtered fluorescence correlation spectroscopy (Dolino et al., 2016; Felekyan et al., 2012).

Why has the PBD evolved to display such dynamics even in quiescent SecA? A major contribution of PBD at this early stage of secretion is to optimize promiscuous preprotein docking on SecA. Although enzymatically quiescent as an ATPase, soluble SecA is still a low-micromolar K_d preprotein receptor and becomes a high-nanomolar to low-micromolar K_d receptor when bound to SecY (Gouridis et al., 2009, 2013). SecA binds hundreds of secretory proteins that differ in size, structural folds, and non-folded states and senses them as bivalent ligands, recognizing both their signal peptides and mature domain patches at different clefts (Chatzi et al., 2017; Sardis et al., 2017; Tsirigotaki et al., 2018). Presumably, PBD positioning "guides" preproteins to productively dock on SecA to proceed to secretion (Sardis et al., 2017).

In contrast to the effect of dimer-to-monomer transitions, nucleotides do not appear to alter intrinsic PBD swiveling detectably. This raises the possibility that, while PBD is inherently dynamic in the catalytically quiescent SecA studied here, nucleotide-driven conformational cues in the helicase ATPase motor (Figure 1, blue and cyan) are not coupled to PBD (magenta) motions and vice versa. This is intriguing since, during catalysis, PBD does exert long-range effects that "break" gate1, a salt bridge in the motor, which prevents it from acquiring elevated ATP turnovers and, moreover, mutations in the motor or the PBD do affect each other's conformation (Karamanou et al., 2007; Keramisanou et al., 2006). Our findings lead us to hypothesize the existence of a sophisticated auto-inhibitory mechanism. SecY docking, which primes SecA for high-affinity preprotein binding and ATP turnover (Gouridis et al., 2013), and preprotein binding (Chatzi et al., 2017; Gelis et al., 2007) are expected to relieve this auto-inhibition and allow ATPase motor/PBD conformational crosstalk.

Whether and how PBD motions contribute mechanistically to actual preprotein translocation through SecYEG remains unknown. We entertain two hypotheses; both assume that PBD oscillates between the 3–4 states identified here. In dimeric SecA, which initially docks on SecYEG (Gouridis et al., 2013), states 2 and 1 predominate. In these states, the PBD forms a tighter PBD-IRA2 clamp and may directly contact translocating chains trapped inside it (Bauer and Rapoport, 2009). PBD may thus (Figure 7) (1) act as a brake, to prevent translocating chain "back-slippage" and control a Brownian "ratchet" allowing forward motion (left) (Allen et al., 2016; Tsirigotaki et al., 2017); or (2) bind to the translocating chain and exert a "pushing" stroke (middle). A third possible role relates to the channel rather than to the exiting chain. PBD contacts directly the large, functionally important cytoplasmic protrusion of SecY (right) (Zimmer et al., 2008) as can be seen in models of SecA bound to two SecY structures (Figure S7). Thus, PBD motions could directly control both the structural dynamics of SecYEG and those of the translocating chain.

SmFRET-derived domain dynamics analyzed here combined with HDX-MS-derived structural dynamics analyses (Sardis et al., 2017; Tsirigotaki et al., 2017, 2018) lay the foundations for quantitative dissection of the functional translocase. SecA offers an interesting example of smFRET-derived structural information in proteins. This is a non-trivial, multi-disciplinary effort, requiring the design and testing of multiple fluorescent

pair derivatives. Compared with other methods, smFRET is uniquely suited to the analysis of membrane-associated systems with short-lived, interconverting states and opens numerous exciting future possibilities.

STAR★METHODS

Detailed methods are provided in the online version of this paper and include the following:

- KEY RESOURCES TABLE
- CONTACT FOR REAGENT AND RESOURCE SHARING
- EXPERIMENTAL MODEL AND SUBJECT DETAILS
- METHOD DETAILS
  - Buffers and Reagents
  - Residue Selection
  - Strains, Genetic Manipulations and Mutagenesis
  - Protein Expression, Purification and Functional Assays
  - Fluorescent Labeling
  - Confocal Multi-parameter Setup
  - FRET Measurements
  - Accessible Volume Simulation
  - Generation of PBD States in SecA and SecA-SecY Models
- QUANTIFICATION AND STATISTICAL ANALYSIS
  - Software
  - Single-Molecule Burst Analysis
  - Fluorescence Correlation Spectroscopy (FCS)
  - Photon Distribution Analysis

SUPPLEMENTAL INFORMATION

Supplemental Information includes seven figures, five tables, and two data files and can be found with this article online at https://doi.org/10.1016/j.str.2018.10.006.

ACKNOWLEDGMENTS

We are grateful to G. Gouridis (Rega Institute, KU Leuven) for discussions. Our research was funded through the Research Foundation Flanders (FWO), grant #G.0B49.15 (to J. Hofkens, J. Hendrix, and S.K.), grants #G0683.15 and #G0A5817.N (to J. Hofkens), large infrastructure grant ZW15_09 GOH6316N (to J. Hofkens and J. Hendrix); grant #G0C6814N RiMembR (to A.E.); the Flemish government through long-term structural funding Methusalem CASAS2, grant #Meth/15/04 (to J. Hofkens); the FWO/F.R.S. - FNRS Excellence of Science-EOS program grant #30550343 (to A.E.); the KU Leuven grant C14/16/053 (to J. Hendrix), the EU (FP7 KBBE.2013.3.6-02: Synthetic Biology towards applications; #613877 StrepSynth to A.E.), and RUN (#RUN/16/001 KU Leuven to A.E.). N.V. acknowledges the Agency for Innovation by Science and Technology in Flanders (IWT) for a doctoral scholarship. V.Z. is an FWO postdoctoral fellow.

AUTHOR CONTRIBUTIONS

N.V. performed protein labeling and all smFRET analysis. S.K. designed genetic constructs, purified proteins, analyzed them by size exclusion/MALS, and performed functional *in vivo* and *in vitro* assays. A.G.P. designed and generated genetic constructs. V.Z. generated and analyzed smFRET-derived SecA models. J. Hendrix set up the MFD-PIE microscope and data analysis pipeline and supervised smFRET experiments. N.V. and A.E. wrote the paper with contributions from J. Hendrix, S.K., V.Z., and A.P. J. Hendrix and S.K. managed the project. J. Hendrix, J. Hofkens, S.K., and A.E. conceived and designed the project. All authors reviewed the manuscript.

DECLARATION OF INTERESTS

The authors declare they have no competing financial interests.

Received: June 1, 2018
Revised: August 27, 2018
Accepted: October 10, 2018
Published: November 21, 2018

REFERENCES

Aitken, C.E., Marshall, R.A., and Puglisi, J.D. (2008). An oxygen scavenging system for improvement of dye stability in single-molecule fluorescence experiments. Biophys. J. *94*, 1826–1835.

Akita, M., Shinkai, A., Matsuyama, S., and Mizushima, S. (1991). SecA, an essential component of the secretory machinery of *Escherichia coli*, exists as homodimer. Biochem. Biophys. Res. Commun. *174*, 211–216.

Allen, W.J., Corey, R.A., Oatley, P., Sessions, R.B., Baldwin, S.A., Radford, S.E., Tuma, R., and Collinson, I. (2016). Two-way communication between SecY and SecA suggests a Brownian ratchet mechanism for protein translocation. Elife *5*. 10.7554/eLife.15598.001.

Antonik, M., Felekyan, S., Gaiduk, A., and Seidel, C.A. (2006). Separating structural heterogeneities from stochastic variations in fluorescence resonance energy transfer distributions via photon distribution analysis. J. Phys. Chem. B *110*, 6970–6978.

Bauer, B.W., and Rapoport, T.A. (2009). Mapping polypeptide interactions of the SecA ATPase during translocation. Proc. Natl. Acad. Sci. U S A *106*, 20800–20805.

Berman, H.M., Westbrook, J., Feng, Z., Gilliland, G., Bhat, T.N., Weissig, H., Shindyalov, I.N., and Bourne, P.E. (2000). The Protein Data Bank. Nucleic Acids Res. *28*, 235–242.

Brewer, C.F., and Riehm, J.P. (1967). Evidence for possible nonspecific reactions between N-ethylmaleimide and proteins. Anal. Biochem. *18*, 248–255.

Chatzi, K.E., Sardis, M.F., Tsirigotaki, A., Koukaki, M., Sostaric, N., Konijnenberg, A., Sobott, F., Kalodimos, C.G., Karamanou, S., and Economou, A. (2017). Preprotein mature domains contain translocase targeting signals that are essential for secretion. J. Cell Biol. *216*, 1357–1369.

Cordes, T., Vogelsang, J., and Tinnefeld, P. (2009). On the mechanism of Trolox as antiblinking and antibleaching reagent. J. Am. Chem. Soc. *131*, 5018–5019.

Cotlet, M., Vosch, T., Habuchi, S., Weil, T., Mullen, K., Hofkens, J., and De Schryver, F. (2005). Probing intramolecular Forster resonance energy transfer in a naphthaleneimide-peryleneimide-terrylenediimide-based dendrimer by ensemble and single-molecule fluorescence spectroscopy. J. Am. Chem. Soc. *127*, 9760–9768.

Dolino, D.M., Rezaei Adariani, S., Shaikh, S.A., Jayaraman, V., and Sanabria, H. (2016). Conformational selection and submillisecond dynamics of the ligand-binding domain of the N-methyl-d-aspartate receptor. J. Biol. Chem. *291*, 16175–16185.

Eggeling, C., Berger, S., Brand, L., Fries, J.R., Schaffer, J., Volkmer, A., and Seidel, C.A. (2001). Data registration and selective single-molecule analysis using multi-parameter fluorescence detection. J. Biotechnol. *86*, 163–180.

Felekyan, S., Kalinin, S., Sanabria, H., Valeri, A., and Seidel, C.A. (2012). Filtered FCS: species auto- and cross-correlation functions highlight binding and dynamics in biomolecules. ChemPhysChem *13*, 1036–1053.

Fiser, A., and Sali, A. (2003). ModLoop: automated modeling of loops in protein structures. Bioinformatics *19*, 2500–2501.

Fiser, A., and Simon, I. (2000). Predicting the oxidation state of cysteines by multiple sequence alignment. Bioinformatics *16*, 251–256.

Förster, T. (1946). Energiewanderung und Fluoreszenz. Naturwissenschaften *33*, 166–175.

Gansen, A., Valeri, A., Hauger, F., Felekyan, S., Kalinin, S., Toth, K., Langowski, J., and Seidel, C.A. (2009). Nucleosome disassembly intermediates characterized by single-molecule FRET. Proc. Natl. Acad. Sci. U S A *106*, 15308–15313.

Gelis, I., Bonvin, A.M., Keramisanou, D., Koukaki, M., Gouridis, G., Karamanou, S., Economou, A., and Kalodimos, C.G. (2007). Structural basis for signal-sequence recognition by the translocase motor SecA as determined by NMR. Cell *131*, 756–769.

Gold, V.A., Whitehouse, S., Robson, A., and Collinson, I. (2013). The dynamic action of SecA during the initiation of protein translocation. Biochem. J. *449*, 695–705.

Gouridis, G., Karamanou, S., Gelis, I., Kalodimos, C.G., and Economou, A. (2009). Signal peptides are allosteric activators of the protein translocase. Nature *462*, 363–367.

Gouridis, G., Karamanou, S., Koukaki, M., and Economou, A. (2010). In vitro assays to analyze translocation of the model secretory preprotein alkaline phosphatase. Methods Mol. Biol. *619*, 157–172.

Gouridis, G., Karamanou, S., Sardis, M.F., Scharer, M.A., Capitani, G., and Economou, A. (2013). Quaternary dynamics of the SecA motor drive translocase catalysis. Mol. Cell *52*, 655–666.

Ha, T., and Tinnefeld, P. (2012). Photophysics of fluorescent probes for single-molecule biophysics and super-resolution imaging. Annu. Rev. Phys. Chem. *63*, 595–617.

Hellenkamp, B., Schmid, S., Doroshenko, O., Opanasyuk, O., Kühnemuth, R., Rezaei Adariani, S., Ambrose, B., Aznauryan, M., Barth, A., Birkedal, V., et al. (2018). Precision and accuracy of single-molecule FRET measurements—a multi-laboratory benchmark study. Nat. Methods *15*, 669–676.

Hendrix, J., and Lamb, D.C. (2013). Pulsed interleaved excitation: principles and applications. Methods Enzymol. *518*, 205–243.

Hofkens, J., Cotlet, M., Vosch, T., Tinnefeld, P., Weston, K.D., Ego, C., Grimsdale, A., Müllen, K., Beljonne, D., Bredas, J.L., et al. (2003). Revealing competitive Forster-type resonance energy-transfer pathways in single bichromophoric molecules. Proc. Natl. Acad. Sci. U S A *100*, 13146–13151.

Huang, B., Wu, H., Kim, S., and Zare, R.N. (2005). Coating of poly(dimethylsiloxane) with n-dodecyl-beta-D-maltoside to minimize nonspecific protein adsorption. Lab Chip *5*, 1005–1007.

Huber, D., Rajagopalan, N., Preissler, S., Rocco, M.A., Merz, F., Kramer, G., and Bukau, B. (2011). SecA interacts with ribosomes in order to facilitate post-translational translocation in bacteria. Mol. Cell *41*, 343–353.

Hunt, J.F., Weinkauf, S., Henry, L., Fak, J.J., Mcnicholas, P., Oliver, D.B., and Deisenhofer, J. (2002). Nucleotide control of interdomain interactions in the conformational reaction cycle of SecA. Science *297*, 2018–2026.

Jomaa, A., Boehringer, D., Leibundgut, M., and Ban, N. (2016). Structures of the *E. coli* translating ribosome with SRP and its receptor and with the translocon. Nat. Commun. *7*, 10471.

Kalinin, S., Felekyan, S., Valeri, A., and Seidel, C.A. (2008). Characterizing multiple molecular states in single-molecule multiparameter fluorescence detection by probability distribution analysis. J. Phys. Chem. B *112*, 8361–8374.

Kalinin, S., Peulen, T., Sindbert, S., Rothwell, P.J., Berger, S., Restle, T., Goody, R.S., Gohlke, H., and Seidel, C.A. (2012). A toolkit and benchmark study for FRET-restrained high-precision structural modeling. Nat. Methods *9*, 1218–1225.

Kapanidis, A.N., Lee, N.K., Laurence, T.A., Doose, S., Margeat, E., and Weiss, S. (2004). Fluorescence-aided molecule sorting: analysis of structure and interactions by alternating-laser excitation of single molecules. Proc. Natl. Acad. Sci. U S A *101*, 8936–8941.

Karamanou, S., Bariami, V., Papanikou, E., Kalodimos, C.G., and Economou, A. (2008). Assembly of the translocase motor onto the preprotein-conducting channel. Mol Microbiol *70*, 311–322.

Karamanou, S., Gouridis, G., Papanikou, E., Sianidis, G., Gelis, I., Keramisanou, D., Vrontou, E., Kalodimos, C.G., and Economou, A. (2007). Preprotein-controlled catalysis in the helicase motor of SecA. EMBO J. *26*, 2904–2914.

Karamanou, S., Vrontou, E., Sianidis, G., Baud, C., Roos, T., Kuhn, A., Politou, A.S., and Economou, A. (1999). A molecular switch in SecA protein couples ATP hydrolysis to protein translocation. Mol. Microbiol. *34*, 1133–1145.

Kellner, R., Hofmann, H., Barducci, A., Wunderlich, B., Nettels, D., and Schuler, B. (2014). Single-molecule spectroscopy reveals chaperone-mediated expansion of substrate protein. Proc. Natl. Acad. Sci. U S A *111*, 13355–13360.

Keramisanou, D., Biris, N., Gelis, I., Sianidis, G., Karamanou, S., Economou, A., and Kalodimos, C.G. (2006). Disorder-order folding transitions underlie catalysis in the helicase motor of SecA. Nat. Struct. Mol. Biol. *13*, 594–602.

Kudryavtsev, V., Sikor, M., Kalinin, S., Mokranjac, D., Seidel, C.A., and Lamb, D.C. (2012). Combining MFD and PIE for accurate single-pair Forster resonance energy transfer measurements. ChemPhysChem *13*, 1060–1078.

Kusters, I., van den Bogaart, G., Kedrov, A., Krasnikov, V., Fulyani, F., Poolman, B., and Driessen, A.J. (2011). Quaternary structure of SecA in solution and bound to SecYEG probed at the single molecule level. Structure *19*, 430–439.

Lamb, D.C., Schenk, A., Rocker, C., Scalfi-Happ, C., and Nienhaus, G.U. (2000). Sensitivity enhancement in fluorescence correlation spectroscopy of multiple species using time-gated detection. Biophys. J. *79*, 1129–1138.

Laurence, T.A., Kwon, Y., Yin, E., Hollars, C.W., Camarero, J.A., and Barsky, D. (2007). Correlation spectroscopy of minor fluorescent species: signal purification and distribution analysis. Biophys. J. *92*, 2184–2198.

Lee, N.K., Kapanidis, A.N., Wang, Y., Michalet, X., Mukhopadhyay, J., Ebright, R.H., and Weiss, S. (2005). Accurate FRET measurements within single diffusing biomolecules using alternating-laser excitation. Biophys. J. *88*, 2939–2953.

Mitchell, C., and Oliver, D. (1993). Two distinct ATP-binding domains are needed to promote protein export by Escherichia coli SecA ATPase. Mol. Microbiol. *10*, 483–497.

Moeyaert, B., Nguyen Bich, N., De Zitter, E., Rocha, S., Clays, K., Mizuno, H., van Meervelt, L., Hofkens, J., and Dedecker, P. (2014). Green-to-red photoconvertible Dronpa mutant for multimodal super-resolution fluorescence microscopy. ACS Nano *8*, 1664–1673.

Müller, B.K., Zaychikov, E., Bräuchle, C., and Lamb, D.C. (2005). Pulsed interleaved excitation. Biophys. J. *89*, 3508–3522.

Nir, E., Michalet, X., Hamadani, K.M., Laurence, T.A., Neuhauser, D., Kovchegov, Y., and Weiss, S. (2006). Shot-noise limited single-molecule FRET histograms: comparison between theory and experiments. J. Phys. Chem. B *110*, 22103–22124.

Papanikolau, Y., Papadovasilaki, M., Ravelli, R.B., McCarthy, A.A., Cusack, S., Economou, A., and Petratos, K. (2007). Structure of dimeric SecA, the *Escherichia coli* preprotein translocase motor. J. Mol. Biol. *366*, 1545–1557.

Pettersen, E.F., Goddard, T.D., Huang, C.C., Couch, G.S., Greenblatt, D.M., Meng, E.C., and Ferrin, T.E. (2004). UCSF Chimera–a visualization system for exploratory research and analysis. J. Comput. Chem. *25*, 1605–1612.

Rapoport, T.A. (2007). Protein translocation across the eukaryotic endoplasmic reticulum and bacterial plasma membranes. Nature *450*, 663–669.

Rasnik, I., McKinney, S.A., and Ha, T. (2006). Nonblinking and long-lasting single-molecule fluorescence imaging. Nat. Methods *3*, 891–893.

Roy, R., Hohng, S., and Ha, T. (2008). A practical guide to single-molecule FRET. Nat. Methods *5*, 507–516.

Sardis, M.F., and Economou, A. (2010). SecA: a tale of two protomers. Mol. Microbiol. *76*, 1070–1081.

Sardis, M.F., Tsirigotaki, A., Chatzi, K.E., Portaliou, A.G., Gouridis, G., Karamanou, S., and Economou, A. (2017). Preprotein conformational dynamics drive bivalent translocase docking and secretion. Structure *25*, 1056–1067.e6.

Schaffer, J., Volkmer, A., Eggeling, C., Subramaniam, V., Striker, G., and Seidel, C.A.M. (1999). Identification of single molecules in aqueous solution by time-resolved fluorescence anisotropy. J. Phys. Chem. A *103*, 331–336.

Schrimpf, W., Barth, A., Hendrix, J., and Lamb, D.C. (2018). PAM: a framework for integrated analysis of imaging, single-molecule and ensemble fluorescence data. Biophys. J. *114*, 1518–1528.

Schuler, B., and Hofmann, H. (2013). Single-molecule spectroscopy of protein folding dynamics–expanding scope and timescales. Curr. Opin. Struct. Biol. *23*, 36–47.

Sianidis, G., Karamanou, S., Vrontou, E., Boulias, K., Repanas, K., Kyrpides, N., Politou, A.S., and Economou, A. (2001). Cross-talk between catalytic and regulatory elements in a DEAD motor domain is essential for SecA function. EMBO J. *20*, 961–970.

Singh, R., Kraft, C., Jaiswal, R., Sejwal, K., Kasaragod, V.B., Kuper, J., Burger, J., Mielke, T., Luirink, J., and Bhushan, S. (2014). Cryo-electron microscopic structure of SecA protein bound to the 70S ribosome. J. Biol. Chem. *289*, 7190–7199.

Studier, F.W., Rosenberg, A.H., Dunn, J.J., and Dubendorff, J.W. (1990). Use of T7 RNA polymerase to direct expression of cloned genes. Methods Enzymol. *185*, 60–89.

Talavera, A., Hendrix, J., Versees, W., Jurenas, D., Van Nerom, K., Vandenberk, N., Singh, R.K., Konijnenberg, A., De Gieter, S., Castro-Roa, D., et al. (2018). Phosphorylation decelerates conformational dynamics in bacterial translation elongation factors. Sci. Adv. *4*, eaap9714.

Tessler, L.A., Reifenberger, J.G., and Mitra, R.D. (2009). Protein quantification in complex mixtures by solid phase single-molecule counting. Anal. Chem. *81*, 7141–7148.

Tomov, T.E., Tsukanov, R., Masoud, R., Liber, M., Plavner, N., and Nir, E. (2012). Disentangling subpopulations in single-molecule FRET and ALEX experiments with photon distribution analysis. Biophys. J. *102*, 1163–1173.

Tsirigotaki, A., Chatzi, K.E., Koukaki, M., De Geyter, J., Portaliou, A.G., Orfanoudaki, G., Sardis, M.F., Trelle, M.B., Jorgensen, T.J.D., Karamanou, S., et al. (2018). Long-lived folding intermediates predominate the targeting-competent secretome. Structure *26*, 695–707.e5.

Tsirigotaki, A., De Geyter, J., Sostaric, N., Economou, A., and Karamanou, S. (2017). Protein export through the bacterial Sec pathway. Nat. Rev. Microbiol. *15*, 21–36.

Vandenberk, N., Barth, A., Borrenberghs, D., Hofkens, J., and Hendrix, J. (2018). Evaluation of blue and far-red dye pairs in single-molecule FRET experiments. J. Phys. Chem. B *122*, 4249–4266.

Vogelsang, J., Kasper, R., Steinhauer, C., Person, B., Heilemann, M., Sauer, M., and Tinnefeld, P. (2008). A reducing and oxidizing system minimizes photobleaching and blinking of fluorescent dyes. Angew. Chem. Int. Ed. *47*, 5465–5469.

Vosch, T., Cotlet, M., Hofkens, J., Van Der Biest, K., Lor, M., Weston, K.D., Tinnefeld, P., Sauer, M., Latterini, L., Müllen, K., et al. (2003). Probing Förster type energy pathways in a first generation rigid dendrimer bearing two perylene imide chromophores. J. Phys. Chem. A *107*, 6920–6931.

Woodbury, R.L., Hardy, S.J., and Randall, L.L. (2002). Complex behavior in solution of homodimeric SecA. Protein Sci. *11*, 875–882.

Wowor, A.J., Yu, D., Kendall, D.A., and Cole, J.L. (2011). Energetics of SecA dimerization. J. Mol. Biol. *408*, 87–98.

Zander, C., Sauer, M., Drexhage, K.H., Ko, D.S., Schulz, A., Wolfrum, J., Brand, L., Eggeling, C., and Seidel, C.A.M. (1996). Detection and characterization of single molecules in aqueous solution. Appl. Phys. B *63*, 517–523.

Zimmer, J., Nam, Y., and Rapoport, T.A. (2008). Structure of a complex of the ATPase SecA and the protein-translocation channel. Nature *455*, 936–943.

Zimmer, J., and Rapoport, T.A. (2009). Conformational flexibility and peptide interaction of the translocation ATPase SecA. J. Mol. Biol. *394*, 606–612.

STAR★METHODS

KEY RESOURCES TABLE

REAGENT or RESOURCE	SOURCE	IDENTIFIER
Antibodies		
Rabbit polyclonal α-SecA	(Karamanou et al., 2008)	N/A
Peroxidase AffiniPure Goat Anti-Rabbit IgG (H+L)	Jackson ImmunoResearch Europe Lt	Code: 111-035-003; RRID: AB_2313567
Bacterial and Virus Strains		
DH5α: F$^-$ *endA1 glnV44 thi-1 recA1 relA1 gyrA96 deoR nupG purB20* φ80d*lacZ*ΔM15 Δ(*lacZYA-argF*)U169, hsdR17($r_K^-m_K^+$), λ$^-$	Invitrogen	Cat#18258012
BL21.19 (DE3) (secA13 (Am) supF (Ts) trp (Am) zch::Tn10 recA::cat clpA::kan)	(Mitchell and Oliver, 1993)	N/A
BL21 (DE3) : *E. coli* str. B F$^-$ *ompT gal dcm lon hsdS$_B$*($r_B^-m_B^-$) λ(DE3 [*lacI lacUV5-T7p07 ind1 sam7 nin5*]) [*malB*$^+$]$_{K-12}$(λ^S)	(Studier et al., 1990); NEB	NEB C2527
T7 express *lys*Y/I^q (DE3) : : MiniF lysY lacIq (CamR) / fhuA2 lacZ::T7 gene1 [lon] ompT gal sulA11 R(mcr73::miniTn10–TetS)2 [dcm] R(zgb-210::Tn10–TetS) endA1 Δ(mcrC-mrr)114::IS10	NEB	NEB C3013
Chemicals, Peptides, and Recombinant Proteins		
Tris base	Sigma-Aldrich	Cat#T1378
NaCl	Sigma-Aldrich	Cat#7647-14-5
Trolox	Sigma-Aldrich	Cat#53188-07-1
BSA	Sigma-Aldrich	N/A
ATTO488-CA	ATTO-TEC GmBH	Cat# AD 488-21
ATTO655-CA	ATTO-TEC GmBH	Cat# AD 655-21
ATTO488-maleimide	ATTO-TEC GmBH	Cat# D 488-45
Alexa Fluor 647 C2-maleimide	Life Technologies Europe BV	Cat#A20347
PFU Ultra Polymerase	Agilent	M7741
DpnI	Promega	R6231
Dithiotheitrol (DTT)	ApplichemPanreac	Cat#A1101
TCEP	Sigma-Aldrich	Cat#51805-45-9
Ethylenediaminetetraaceticacid, diNa salt, 2aq (EDTA)	Chemlab	Cat#CL00.0503
HEPES	Fisher	Cat#BP310
Imidazole	Carl Roth	Cat# 3899
Glycerol	Sigma-Aldrich	Cat#56-81-5
Phenylmethylsulfonylfluoride (PMSF)	Roth	Cat#6367
Magnesium Chloride ($MgCl_2$)	Roth	Cat#2189
Isopropylβ-D-1-thiogalactopyranoside (IPTG)	FischerScientific	Cat#BP1755
Critical Commercial Assays		
Site-directed mutagenesis protocol	Stratagene-Agilent	N/A
Plasmid purification (NucleoSpin® Plasmid EasyPure)	Macherey- Nagel	Cat# 740727
Deposited data		
Escherichia coli SecA, the preprotein translocase dimeric ATPase	(Papanikolau et al., 2007)	PDB: 2FSF
Crystal structure of the protein-translocation complex formed by the SecY channel and the SecA ATPase	(Zimmer et al., 2008)	PDB: 3DIN
Crystal structure of the SecA translocation ATPase from *Bacillus subtilis*	(Hunt et al., 2002)	PDB: 1M6N

(*Continued on next page*)

Continued

REAGENT or RESOURCE	SOURCE	IDENTIFIER
Solution structure of the SecA-signal peptide complex	(Gelis et al., 2007)	PDB: 2VDA
RNC in complex with a translocating SecYEG	(Jomaa et al., 2016)	PDB: 5GAE
Oligonucleotides		
For primers used in this study see Table S4		
Recombinant DNA		
For vectors used in this study see Table S3	This study	N/A
For genetics constructs used in this study see Table S3	This study	N/A
Software and Algorithms		
FPS software	(Kalinin et al., 2012)	http://www.mpc.hhu.de/software/fps.html
PyMol Molecular Graphics system, Version 2.07	Schrödinger	http://www.pymol.com
ModLoop	(Fiser and Sali, 2003)	https://modbase.compbio.ucsf.edu/modloop/
PAM	(Schrimpf et al., 2018)	http://www.cup.uni-muenchen.de/pc/lamb/software/pam.html
RSCB, Protein Data Bank	(Berman et al., 2000)	http://www.rcsb.org/
Other		
Nunc Lab-Tek Chambered cover-glass	Thermofisher Scientific	Cat#155411
0.45 μm filter, reg. cellulose 0.45μm	Grace discovery sciences	Cat#5123260(k45)
PD-10 desalting columns	GE Healthcare Europe GmbH	Cat#17085101
Amicon ultrafiltration columns (50 kDa, Ultra-0.5)	Merck Chemicals	Cat#UFC505024
Amicon ultrafiltration columns (3K, Ultra-15))	Merck Millipore	Cat#UFC900396
Ni^{+2}-NTA Agarose resin	Qiagen	Cat#30250
Hi-Load Superdex 200 26/60 gel filtration column	GE, Healthcare	Cat#28989336
SecA ATP hydrolysis experiment	(Chatzi et al., 2017)	N/A

CONTACT FOR REAGENT AND RESOURCE SHARING

Additional information or requests for resources and reagents should be directed to the Lead Contact, Anastassios Economou (tassos.economou@kuleuven.be).

EXPERIMENTAL MODEL AND SUBJECT DETAILS

For protein purification, *E. coli* BL21 or T7 express *lys*Y/I^q cells transformed with pET3a plasmids carrying *secA* (P10408) or derivatives were grown in 5 L flasks (LB 2.5 L; 30°C; OD_{600} 0.5-0.6). In each case, gene expression was induced (0.2 mM IPTG; 3 h; 30°C. Cells were collected (5,000 g; 4°C; 15 min; Avanti J-26S XPI, JLA 8.1000 rotor; Beckman), resuspended in 50 mM Tris/HCl pH 8; 1 M NaCl; 5% (V/V) glycerol; lysed by using a French press (8,000 psi; 55,16 MPa); 3-5 passes; pre-cooled cylinder at 4°C; Thermo).

METHOD DETAILS

Buffers and Reagents

Tris buffer consists of 50 mM Tris (Sigma-Aldrich, Diegem, Belgium) and 50 mM NaCl (Sigma-Aldrich, Diegem, Belgium) at pH 7. Aged PBS/Trolox buffer was made by dissolving 1 mM Trolox (6-Hydroxy-2,5,7,8-tetramethylchromane-2-carboxylic acid, 543353, Sigma Aldrich, Denmark) overnight (~16 h) at 4°C in the buffer. Prior to experiments, coverslips (Nunc Lab-Tek Chambered cover-glass, 155411, ThermoFisher Scientific, Ghent, Belgium) were coated with 1 mg/mL bovine serum albumin (BSA, Sigma-Aldrich, Diegem, Belgium). The BSA stock solution was made by dissolving 10 mg/mL BSA in PBS, passing the solution through a 0.45 μm filter (Reg. cellulose 0.45 μm, 5123260(K45), Grace discovery sciences, Deerfield, IL, USA.) the solution and subsequent flash freezing aliquots that were stored at -20°C. The free dyes that were used for microscope calibration are Atto488 (ATTO 488-CA, ATTO-TEC GmbH, Siegen, Germany) and Atto655 (ATTO 655-CA). The dyes that were used for labeling the protein are ATTO 488 maleimide (ATTO-TEC GmbH, Siegen, Germany) and Alexa Fluor 647 C_2-maleimide (Life Technologies Europe BV, Gent, Belgium). Dye properties are summarized in Table S1.

Residue Selection

Six selection criteria were applied for specific residue selection. These residues should: (a) localize on secondary structure elements (α-helix or β-sheet). This way, dye to dye distances would report on protein conformational changes and not local wobble effects. (b) have good solvent accessibility. As dyes are not infinitely small, labeling of surface residues increases labelling efficiency and reduces steric interference. Accessible volumes were calculated using the FRET-restrained positioning and screening (FPS) software (Kalinin et al., 2012) to build models of the expected FRET distances in soluble SecA and to model dye motion in space at specific residues (Figure S1D). (c) not participate in hydrogen bonding or interactions with neighboring residues. This avoids placing the dyes on residues with direct structural roles. (d) not participate in the SecA dimerization or the SecY-binding or the preprotein binding interfaces (e) be located such that the change in FRET between 2 residues from one PBD conformation to another (Figure 1A) is high. FRET changes can be calculated from the actual space-averaged distance between the dyes, attached to a cysteine residue via a ~20 Å linker. (f) be located such that the attached dyes do not collide or sterically hinder one another. Using the above criteria, we selected 31 FRET pairs (Table S2).

Strains, Genetic Manipulations and Mutagenesis

We used the fully functional SecA(cys$^-$) that has its 4 cysteinyl residues substituted (Chatzi et al., 2017; Sardis et al., 2017) (positions 98, 885, 887 and 896) substituted by serine (C98S) or alanines (885, 887 and 896). Gene-mutations were introduced by following the QuickChange Site-Directed Mutagenesis protocol (Stratagene-Agilent); templates and primers are listed in Tables S3 and S4. For PCR mutagenesis PFU Ultra Polymerase (Agilent) was used; DpnI was used to cleave the maternal methylated DNA (Promega). All PCR-generated plasmids were sequenced (Macrogen, Europe). Plasmids were stored in DH5α cells.

Protein Expression, Purification and Functional Assays

Gene-overexpression was induced using BL21 (DE3; NEB C2527) (Studier et al., 1990) or T7 express *lys*Y/I^q (DE3; NEB C3013). Bacteria growth conditions, purification of SecA or mutant derivatives, size exclusion chromatography in line with MALS, *in vivo* complementation of with *secA* or derivatives and SecA ATP hydrolysis activity measurement *in vitro* was performed as previously described (Chatzi et al., 2017; Gouridis et al., 2013; Karamanou et al., 2007).

Fluorescent Labeling

Oxygen was removed from the buffer (50 mM Tris pH 7.0, 50 mM NaCl, termed 'Tris buffer') under vacuum and continuous stirring. TCEP was removed from the protein solution by gel filtration (PD-10 desalting columns, GE Healthcare Europe GmbH, Diegem, Belgium) and the protein was concentrated to at least 30 μM by ultrafiltration (Nominal molecular weight limit = 50 kDa Amicon Ultra-0.5, Merck Chemicals N.V., Overijse, Belgium) at 14,000 g and 4°C. An equal molar amount (60 μM) of ATTO 488 maleimide (ATTO-TEC GmbH, Siegen, Germany) and Alexa Fluor 647 C_2-maleimide (Life Technologies Europe BV, Gent, Belgium) was mixed, the protein was added to a final concentration of 50 μM and samples were kept overnight at 4°C. Free dye was removed by gel filtration and ultrafiltration. A representative labeling result is presented in Figure S3C (DTT condition). The ATTO488-maleimide typically exhibited 30-50 % higher labeling efficiency than the Alexa Fluor 647-maleimide. This might be attributed to the dye's differences in charge (ATTO 488: 1+; Alexa Fluor 647: 4-/1+), size (ATTO 488: 710Da; Alexa Fluor 647: ~1250Da) or structure. Typically, 20-50 % of the proteins were labelled by both dyes. According to our experience, protein concentration prior to labeling, the batch of the dye, the degree of reduction of the Cys-SH moiety and the time between protein purification and labelling, all influenced this percentage. However, since FRET experiments were carried out using alternating FRET donor and acceptor excitation, the presence of both dyes can be verified per passing molecule; thus, the resulting FRET histograms represent the 100% of doubly labeled molecules. Tris buffer containing 50% (V/V) glycerol was added 1:1 and the labeled protein sample was divided in aliquots and the samples were stored at -20°C.

Confocal Multi-parameter Setup

For all ensemble and single-molecule experiments, a home-built multi-parameter fluorescence detection microscope with pulsed interleaved excitation (MFD-PIE, (Kudryavtsev et al., 2012)) was used (see scheme of the setup in Figure S1A). Two lasers were used: a pulsed 483-nm laser diode and a 635-nm laser diode, alternated at 26.67 MHz and delayed ~18 ns with respect to each other. The power density inside the focus was calculated via:

$$\text{Power density}\left[\text{kW}/\text{cm}^2\right] = 0.04\frac{P}{\pi\omega_r^2}, \qquad \text{(Equation 1)}$$

where P is the laser power (in μW) measured in between the excitation polychroic mirror and the objective lens and ω_r is the lateral focus waist (in μm). Furthermore, the equation assumes that 40% of the measured light reaches the sample. Sample emission was transmitted through a pinhole and spectrally split. Both, the blue range and red range were split by polarization on two detection channels. Photons were detected on four avalanche photodiodes: $B_{\parallel}$ (blue-parallel), $B_{\perp}$ (blue-perpendicular), $R_{\parallel}$ (red-parallel) and $R_{\perp}$ (red-perpendicular) (Figure S1B), which were connected to a time-correlated single photon counting (TCSPC) device. Signals from each TCSPC channel were divided in time gates (Lamb et al., 2000) to discern 483-nm excited FRET photons from 635-nm excited acceptor photons: $BB_{\parallel}$, $BB_{\perp}$, $BR_{\parallel}$, $BR_{\perp}$, $RR_{\parallel}$, $RR_{\perp}$ (Figure S1B). Microscope alignment (excitation light guiding, objective lens correction collar, pinhole, detectors) and determination of the lateral (ω_r) and axial (ω_z) focus waists were done using real-time

fluorescence correlation spectroscopy (FCS, see further) on freely diffusing ATTO488-COOH and ATTO655-COOH in water. For more details about the used equipment the reader is referred to (Vandenberk et al., 2018).

FRET Measurements

The labeled protein was diluted in Tris buffer containing 1 mM aged Trolox (Cordes et al., 2009) up to a concentration of 100-200 pM. Trolox efficiently prevented the protein from adsorbing to the sample holder, thereby decreasing the overall measurement time, yet had no influence on the functionality of the molecule, corroborated by identical FRET histograms in absence or presence of Trolox (Figure S2G, right). Coverslips (Nunc Lab-Tek Chambered Coverglass, ThermoFisher Scientific BVBA, Erembodegem, Belgium) were pre-coated with 1 mg/mL bovine serum albumin (BSA) and washed twice with the sample solution, after which 30 μL of the sample solution was added. Adding other agents to the sample solution such as BSA (Tessler et al., 2009) or the non-ionic detergent, n-Dodecyl-β-BD-maltopyranoside (DDM) (Huang et al., 2005) were also tested, but a significant improvement was only seen for Trolox and DDM. Various coatings of coverslips (with Fibronectin, Laminin, Collagen or BSA) were also tested without improvement compared to BSA (data not shown). Unless explicitly stated otherwise, smFRET experiments were performed during at least 1 hour at 100 μW 483 nm and 50 μW of 635 nm excitation at room temperature (22°C). Background and scatter information was obtained via a buffer measurement under identical condition. The background/scatter information is needed for obtaining absolute E (Equation 2) and S (Equation 3) parameters, but also for correct lifetime and PDA analysis (described later). Unless explicitly stated otherwise, all burst measurements were performed during at least 1 hour at 100 μW of 483 nm excitation and 50 μW of 635 nm excitation.

Accessible Volume Simulation

The geometry of the donor and acceptor dyes, including the linker length (measured from the C5 of Thymidine to the geometrical center of the dye), linker width and 3D radius was obtained from the FPS manual (Kalinin et al., 2012). The different parameters are summarized in Table S1. The FPS tool (Kalinin et al., 2012) was used to simulate the accessible volume per dye in the context of the actual dsDNA, using standard settings (i.e. search nodes = 3, clash tolerance = 1.0 Å). This information, together with R_0 (54.7 Å), was used to estimate the simulated FRET averaged D/A distance, $\langle R_{DA} \rangle_E$.

Generation of PBD States in SecA and SecA-SecY Models

Starting structures used to generate the SecA models were 3DIN, 2VDA and 1M6N, which correspond to close, open and wide-open states of the PBD, respectively. The PBD (230-370 a.a.) from 2VDA was used and treated as rigid body to model the different smFRET states (state 1, 2, 2A and 3). To generate the state 2A and satisfy the smFRET distances, the PBD and part of the Stem had to be used and re-positioned (216-377 a.a.). All the PBDs movements and re-localization were restrained based on the smFRET probes distances in PyMol (The PyMOL Molecular Graphics System, Version 2.0.7 Schrödinger, LLC). To obtain a single set of coordinates, the PBDs were merged to the stem using ModLoop (Fiser and Sali, 2003; Fiser and Simon, 2000). The 3DIN structure from *Thermotoga maritima* was used to model the closed helicase ATPase motor on *Escherichia coli* SecA based on superposition. Similarly, the 3DIN structure was also used to generate the SecA-SecY complexes, where the SecA is the monomeric State 2A aligned to the 3DIN SecA in complex with SecY. In this model, the 3DIN SecY remains unaltered. Alternatively, and based on superposition with the latter model, a SecA-SecY model comprising *E. coli*-only components was generated. The 5GAE SecY structure was used. All the models were energy minimized using Chimera (Pettersen et al., 2004).

QUANTIFICATION AND STATISTICAL ANALYSIS

Software

All simulations and analyses of experimental data were performed in the software package PAM (Schrimpf et al., 2018). The software is available as source code, requiring MATLAB to run, or as pre-compiled standalone distributions for Windows or MacOS at http://www.cup.uni-muenchen.de/pc/lamb/software/pam.html or hosted in Git repositories under http://www.gitlab.com/PAM-PIE/PAM and http://www.gitlab.com/PAM-PIE/PAMcompiled. Sample data is provided under http://www.gitlab.com/PAM-PIE/PAM-sampledata. A detailed manual is found under http://pam.readthedocs.io.

Single-Molecule Burst Analysis

Burst Identification

For single-molecule data, a two-color MFD all-photon burst search algorithm (Nir et al., 2006) using a 500 μs sliding time window (min. 50 photons per burst, min. 5 photons per time window) and a kernel-density estimator (ALEX-2CDE < 15, (Tomov et al., 2012)) were used to identify single donor-acceptor labeled molecules in the fluorescence trace. Data was further thresholded using a $|T_{fret}-T_{red}|<0.07$, to remove bursts (typically 10%) exhibiting photobleaching during molecule passage (Kudryavtsev et al., 2012). Additionally, a 0-20-ms burst duration cut was applied to remove sparse (< 1%) slow moving long aggregates, since these can significantly bias time window based analyses such as PDA.

FRET Efficiency

The absolute burst-averaged FRET efficiency E was calculated with:

$$E = \frac{F_{BR} - \alpha F_{RR} - \beta F_{BB}}{F_{BR} - \alpha F_{RR} - \beta F_{BB} + \gamma F_{BB}}, \quad \text{(Equation 2)}$$

where $F_{BR} = S_{BR} - B_{BR}$ is the background corrected number of photons in both red detection channels after blue excitation (with S_{BR} and B_{BR} the summed intensity and background, respectively, in time gates $BR_{\parallel}$ and $BR_{\perp}$); $F_{BB} = S_{BB} - B_{BB}$ the background corrected number of photons in the blue detection channel after blue excitation (with S_{BB} and B_{BB} the summed intensity and background, respectively, in time gates $BB_{\parallel}$ and $BB_{\perp}$), $F_{RR} = S_{RR} - B_{RR}$ the background corrected number of photons in the red detection channel after red excitation (with S_{RR} and B_{RR} the summed intensity and background, respectively, in time gates $RR_{\parallel}$ and $RR_{\perp}$), α a correction factor for direct excitation of the acceptor with the 483 nm laser, β a correction factor for emission crosstalk of the donor in the acceptor channel, and γ the relative detection efficiency of the donor and acceptor (Kudryavtsev et al., 2012).

Stoichiometry

The corrected stoichiometry ratio S was calculated with:

$$S = \frac{F_{BR} - \alpha F_{RR} - \beta F_{BB} + \gamma F_{BB}}{F_{BR} - \alpha F_{RR} - \beta F_{BB} + \gamma F_{BB} + F_{RR}}, \quad \text{(Equation 3)}$$

resulting in the ratio of the blue laser excited photons over all excited photons (blue and red laser). According to this calculation, D-only labeled molecules will have S values near unity, while A-only labeled molecules will have values near zero. Double labeled-molecules will exhibit S values between 0.2-0.6 depending on the used dya pair, the microscope and the laser power ratio.

Data Correction

First, background was subtracted from the experimental signals. Then, the β- and α-factors were determined directly from the measurement (Kudryavtsev et al., 2012) and data was corrected. Finally, the center values of the E-S data cloud for each protein were estimated manually, plotted in an E vs. $1/S$ graph, and a straight line was fitted to the resulting data to obtain the γ-factor:

$$\gamma = \frac{\Omega - 1}{\Omega + \Sigma - 1}, \quad \text{(Equation 4)}$$

where Ω is the intercept and Σ the slope of the linear fit.

Distances

FRET-averaged D/A distances (Kalinin et al., 2012) were obtained from the center E values with:

$$\langle R_{DA} \rangle_E = R_0 \left(\frac{1 - E}{E} \right)^{1/6}, \quad \text{(Equation 5)}$$

where R_0 is the Förster distance (54.7 Å), that was calculated using the measured dye spectra (Vandenberk et al., 2018), a refractive index $n = 1.33$, an orientation factor $\kappa^2 = 2/3$, a measured donor quantum yield $\Phi = 0.6$ for Atto488 and acceptor extinction coefficient (ε = 265,000 $cm^{-1}M^{-1}$) (Table S1). The quantum yield was determined using a home-built absorbance/fluorescence spectroscope (Moeyaert et al., 2014). For simplicity, R_{DAE} will be noted R throughout the text.

Burstwise Fluorescence Lifetime

A maximum likelihood estimator approach (MLE, (Schaffer et al., 1999)) was used to estimate single-molecule burst-averaged single-exponential fluorescence lifetimes of the FRET donor, $\tau_{D(A)}$, and FRET acceptor, τ_A. For molecules that are conformationally static during transit through the laser focus, the FRET efficiency is related to the fluorescence lifetime of the donor as follows:

$$E_{static} = 1 - \frac{\tau_{D(A)}}{\tau_D}. \quad \text{(Equation 6)}$$

However, dyes are attached to the molecule of interest via flexible dye linkers, resulting in a Gaussian D/A distance distribution, even for conformationally static molecules. Especially at short distances (high FRET), this effect causes a non-linear relation between the intensity-based E and $\tau_{D(A)}$. We simulated this 'static FRET line including linker dynamics' as follows: we calculated m values for R between 0 and $3 \times R_0$. For every R, we calculated a Gaussian distribution of p distances around the central R, with the apparent linker length as the standard deviation, resulting in a list of m^*p values for R. For every R, we calculated which donor fluorescence lifetime would be associated with it (Equation 6, with τ_D the mean burstwise lifetime of raw burst data with $S > 0.8$). The apparent linker length (6 Å) was obtained from a sub-ensemble donor fluorescence lifetime fitting of double-labeled molecules using a gaussian distance distribution model. Finally, we calculated the species-weighted average lifetime, and from it the intensity-based E (the y-axis of the static FRET line) and the intensity-weighted average lifetime (x-axis of the static FRET line).

Similarly, for molecules exhibiting multiple lifetimes during transit due to conformational FRET dynamics, the burst-averaged lifetime will be fluorescence-weighted towards the long-lifetime species that emits more photons, resulting in an even further rightward shift of the experimental data from the theoretical line (Equation 6).

Burstwise steady-state fluorescence anisotropies of the FRET donor (r_D) and FRET acceptor (r_A) were calculated from the respective fluorescence intensities:

$$r = \frac{GF_{\parallel} - F_{\perp}}{GF_{\parallel} + 2F_{\perp}}, \quad \text{(Equation 7)}$$

where G is the correction factor for the different detection efficiencies in the two polarization channels, $F_{\parallel}$ the intensity in time gate $BB_{\parallel}$ or $RR_{\parallel}$ and $F_{\perp}$ the intensity in time gate $BB_{\perp}$ or $RR_{\perp}$. Perrin equations were calculated with:

$$r = \frac{r_0}{(1 + \tau/\theta)}, \quad \text{(Equation 8)}$$

where r is the single molecule steady state anisotropy, $r_0 = 0.4$ the fundamental anisotropy, τ the fluorescence lifetime and θ the rotational correlation time.

Fluorescence Correlation Spectroscopy (FCS)

Raw data FCS was performed by cross-correlating parallelly and perpendicularly polarized photon streams from any combination of time gates. Subensemble FCS was performed by selecting particular subpopulations in burst space, correlating each burst after adding 10 ms of data before and after, and averaging the resulting data (Laurence et al., 2007). Burstwise diffusion times τ_{diff} were obtained by fitting individual burst correlations with:

$$G(\tau) = \left(1 + \frac{\tau}{\tau_{diff}}\right)^{-1}, \quad \text{(Equation 9)}$$

from which the diffusion coefficient D ($\mu m^2/s$) was calculated:

$$D = \frac{\omega_r^2}{4\tau_D}. \quad \text{(Equation 10)}$$

Photon Distribution Analysis

Photon distribution analysis (PDA) provides a complete statistic description of single-molecule burst experiments, allowing to discern between molecular conformational heterogeneity and any other effects (shot noise, acceptor photophysics, background…) that broaden experimental FRET histograms (Antonik et al., 2006). Here, we used an implementation that models a sum of gaussian distance distributions to the experimental data (Antonik et al., 2006). Practically, burst data was binned into constant time bins (0.2-1 ms) and first thresholded in E_{PR} (Equation 11) vs. S_{PR} (uncorrected stoichiometry) space to remove bins with complex acceptor photophysics or photobleaching. Then, only bins with at least 20 (for displaying purposes) and maximally 250 photons (to reduce calculation time) were analyzed. For displaying purposes, uncorrected proximity ratio histograms were used:

$$E_{PR} = \frac{S_F}{S_D + S_F}, \quad \text{(Equation 11)}$$

where S_D and S_F are the raw photon counts in the donor and FRET channels, respectively. For PDA analysis, data was γ- ($\sim$0.8), β- ($\sim$0.01) and direct acceptor excitation ($\sim$0.01) corrected, and background (0-1.5 kHz) was explicitly taken into account. Correction parameters were determined as described previously (Kapanidis et al., 2004; Kudryavtsev et al., 2012). Unless explicitly stated otherwise, only the 1-ms binned data was used for PDA. Model parameters were optimized using a reduced-χ^2-guided simplex search algorithm. The resulting parameters were the mean FRET-averaged distance R and standard deviation (σ_R) of each Gaussian distributed substate, and, in the case of multiple states, their area fraction A (%). Where possible, different datasets were analyzed simultaneously by optimizing relevant parameters (e.g. area fraction) globally over all datasets to increase fitting robustness. The reader is referred to Figure S5 and Data S2 for an exemplary analysis. Finally, the standard deviation of the distance distributions was globally optimized as a fraction F of the corresponding distance to further improve fitting robustness ($\sigma_R \approx 0.12 \times R$), which has been shown before to be reasonable for FRET experiments with a blinking FRET acceptor (Kalinin et al., 2008, 2012). We have validated this global fitting approach experimentally before with a dataset of nine conformational static dsDNA molecules with different D-A distances (Vandenberk et al., 2018). Interestingly, relative to these control experiments, we did notice a slightly larger F value for SecA (data not shown), which could be indicative of fast exchange dynamics. Criteria for a good fit were a low (< 3) reduced χ^2 value, as well as a weighted residuals plot free of trends. The uncertainty on A was calculated as the standard deviation from at least three independent experiments. The uncertainty on R (Figures 3C and 4C) was calculated in two ways: (i) via error propagation using partial derivatives of Equation 5, the uncertainty on E (as determined using a γ-factor 0.7-0.9) and the uncertainty on R_0 (as determined before for the same dye pairs (Vandenberk et al., 2018)) as input, and (ii) via the standard deviation on R between at least three independent experiments. The reported errors in Figures 3 and 4 are the root mean squares of both values. To display the result, the gaussian substates and their sum was plotted onto the experimental E_{PR} histogram. Probability density functions (PDF) were additionally calculated per state using the A, R and σ_R parameters obtained from PDA. The summed PDF was scaled to a total area of unity, with each state's PDF area corresponding to the fraction of molecules in that state.